Available online at www.sciencedirect.com
ScienceDirect
Tetrahedron: Asymmetry
Tetrahedron: *Asymmetry* 17 (2006) 3248–3264

Development of novel brush-type chiral stationary phases based on terpenoid selectors: HPLC evaluation and theoretical investigation of enantioselective binding interactions

Cristina Moiteiro,[a,*] Nelson Fonseca,[b] Maria J. M. Curto,[a] Regina Tavares,[a] Ana M. Lobo,[c] Paulo Ribeiro-Claro,[b] Vitor Félix[b,*] and Michael G. B. Drew[d]

[a]*INETI, Instituto National de Engenharia, Tecnologia e Inovação I.P., Estrada do Paço do Lumiar, 1649-038 Lisboa, Portugal*
[b]*Departamento de Química, CICECO, Universidade de Aveiro, 3810-193 Aveiro, Portugal*
[c]*Departamento de Química, Centro de Química Fina e Biotecnologia Requinte, Sintor-Uninova, Faculdade de Ciências e Tecnologia, UNL, 2829-516 Monte de Caparica, Portugal*
[d]*School of Chemistry, University of Reading, Whiteknights, Reading RG6 6AD, UK*

Received 23 October 2006; accepted 23 November 2006

Abstract—The terpenoid chiral selectors dehydroabietic acid, 12,14-dinitrodehydroabietic acid and friedelin have been covalently linked to silica gel yielding three chiral stationary phases **CSP 1**, **CSP 2** and **CSP 3**, respectively. The enantiodiscriminating capability of each one of these phases was evaluated by HPLC with four families of chiral aromatic compounds composed of alcohols, amines, phenylalanine and tryptophan amino acid derivatives and β-lactams. The **CSP 3** phase, containing a selector with a large friedelane backbone is particularly suitable for resolving free alcohols and their derivatives bearing fluorine substituents, while **CSP 2** with a dehydroabietic architecture is the only phase that efficiently discriminates 1,1′-binaphthol atropisomers. **CSP 3** also gives efficient resolution of the free amines. All three phases resolve well the racemates of *N*-trifluoracetyl and *N*-3,5-dinitrobenzoyl phenylalanine amino acid ester derivatives. Good enantioseparation of β-lactams and *N*-benzoyl tryptophan amino acid derivatives was achieved on **CSP 1**.

In order to understand the structural factors that govern the chiral molecular recognition ability of these phases, molecular dynamics simulations were carried out in the gas phase with binary diastereomeric complexes formed by the selectors of **CSP 1** and **CSP 2** and several amino acid derivatives. Decomposition of molecular mechanics energies shows that van der Waals interactions dominate the formation of the diastereomeric transient complexes while the electrostatic binding interactions are primarily responsible for the enantioselective binding of the (*R*)- and (*S*)-analytes. Analysis of the hydrogen bonds shows that electrostatic interactions are mainly associated with the formation of N–H···O=C enantioselective hydrogen bonds between the amide binding sites from the selectors and the carbonyl groups of the analytes. The role of mobile phase polarity, a mixture of *n*-hexane and propan-2-ol in different ratios, was also evaluated through molecular dynamics simulations in explicit solvent.

1. Introduction

The enantiomers of chiral compounds with recognised biological activity usually exhibit different physiological effects following different pathways in biological processes.[1,2] Thus, optical resolution of racemic synthetic compounds is one of the most interesting challenges for a synthetic chemist and is essential in several research fields such as pharmaceutical, agrochemical and food chemistry.[2] Over the last two decades an intensive search for novel chiral stationary phases (CSP) for high-performance liquid chromatography (HPLC) has been carried out and CSPs generated from cyclodextrines,[3,4] polysaccharide derivatives,[5] proteins,[6] macrocyclic antibiotics,[7–9] synthetic polymers,[10,11] chiral crown ethers[12] and low molecular weight optically active compounds are already available on the market.[13,14] The latter ones, denominated brush-type or Pirkle-type, are very attractive types to be used in the molecular design of novel phases with enhanced chiral discrimininating ability. Indeed, chiral selectors can be selectively modified allowing a prompt evaluation of the structural changes on the enantioselective recognition process.[15,16] On the other

* Corresponding authors. Tel.: +351 210924751; fax: +351 217168100 (C.M.); e-mail addresses: cristina.moiteiro@ineti.pt; vfelix@dq.ua.pt

0957-4166/$ - see front matter © 2006 Elsevier Ltd. All rights reserved.
doi:10.1016/j.tetasy.2006.11.036

hand, these phases can be produced using selectors obtained directly from the natural chiral pool such as amino acids,[16] alkaloids,[14,17–22] sterols,[14,23–25] and tartaric acid derivatives.[26,27]

Herein we report novel brush-type phases containing chiral selectors derived from natural sources, dehydroabietic acid **1** and friedelin **3**, anchored onto a solid support of silica gel. Both compounds exhibit different functionalities assembled in a rigid skeleton, which allows the chiral molecular recognition of a wide range of organic substrates. Dehydroabietic acid **1** is available in large amounts from the dehydrogenated commercial resin of the pines extracted from *Pinus pinaster*.[28] Friedelin **3** can be obtained from the cork smoker wash solids, which are a by-product generated in large amount by the cork processing industry associated with *Quercus suber* L.[29] Furthermore, this black wax has not yet found a practical application and represents an environmental problem. Both species are widespread in Portuguese forests, one of the most important renewable sources of biomass available in the country for industrial proposes including the production of energy.[30] In an attempt to find other potential applications for these inexpensive natural raw materials with a well recognised high trade value, dehydroabietic acid **1**, 12,14-dinitrodehydroabietic acid **2** and friedelin **3** were selected as chiral selectors of three novel brush-type phases shown in Figures 1 and 2. Selector **2** was obtained by the nitration of **1**.[31] Subsequently, selectors **1**, **2** and **3** were covalently linked to a silica gel support using the larger spacer, 10-undecenylamine, leading to **CSP 1**, **CSP 2** and **CSP 3** phases.[32] Herein we report the synthesis and the structural characterisation of these novel phases. The enantioselective chromatographic resolution capability of these phases was evaluated by HPLC with four sets of aromatic compounds composed of a representative number of alcohols, amines, amino acid derivatives and *cis*-β-lactams (Chart 1).

In order to understand the accumulated chromatographic resolution data at a molecular level, the structural features associated with the chiral recognition modes, molecular modelling studies were carried out on the diastereomeric binding associations formed between the chiral selectors of **CSP 1** and **CSP 2** phases and the analytes of phenylalanine amino acid derivatives **17a** and **17d**. This theoretical investigation comprised of molecular mechanics (MM) energy calculations and molecular dynamics (MD) simulations in the gas phase. The effect of an enhancement of the mobile phase polarity on the enantioselective separation of the amino acid **17a** on **CSP 2** was also evaluated through MD simulations in solution.

2. Results and discussion

2.1. Synthesis of the chiral stationary phases

12,14-Dinitrodehydroabietic acid **2** was synthesised by the introduction of two nitro groups at the 12- and 14-positions of dehydroabietic acid **1** via electrophilic aromatic substitution. These two chiral selectors contain a rigid framework incorporating an aromatic ring and a carboxyl group at the C-4 position, which was used for the covalent link to the silica gel support.

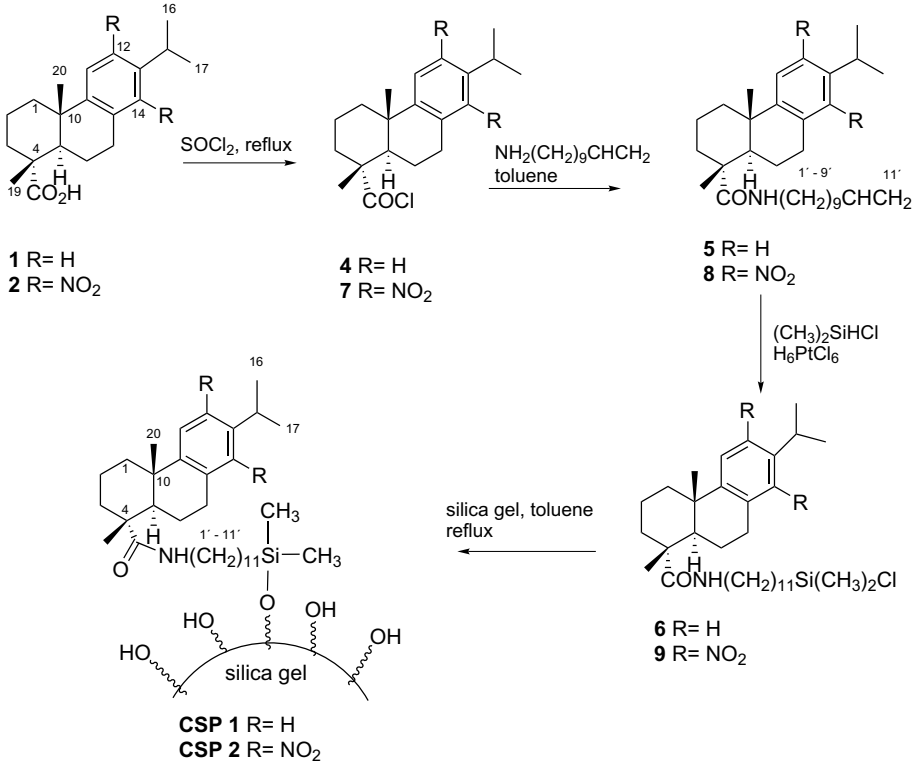

Figure 1. Syntheses of **CSP 1** and **CSP 2** diterpenoid brush-type phases.

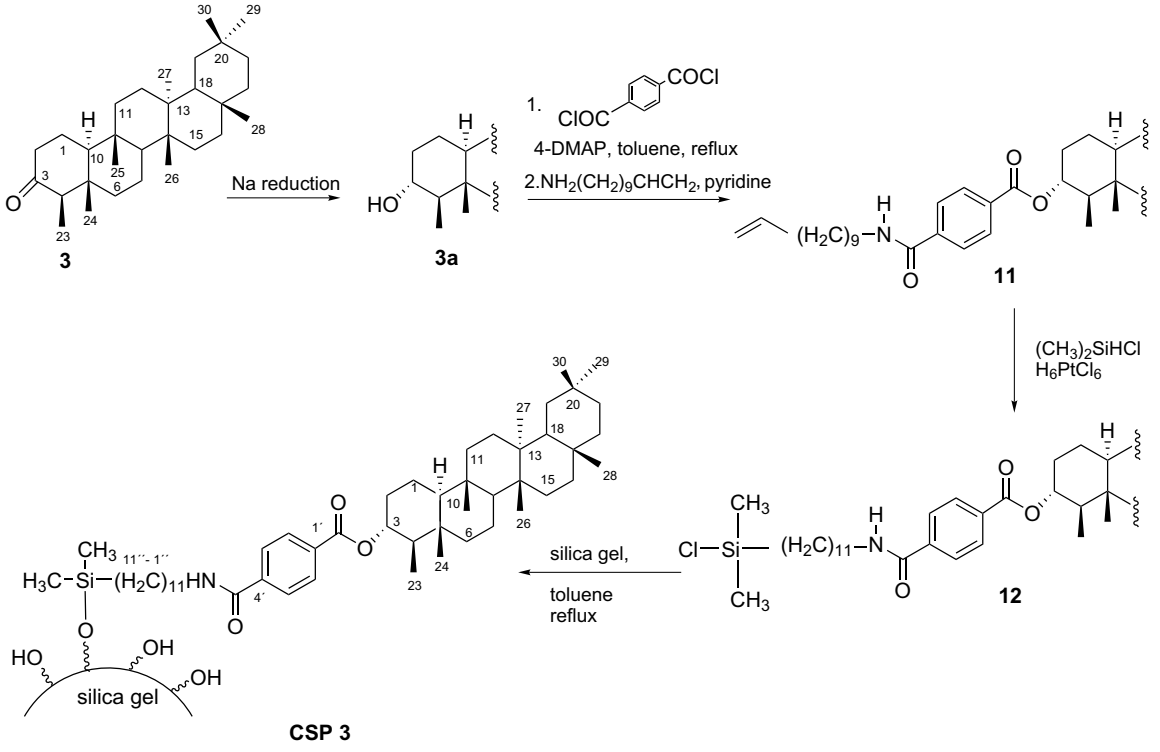

Figure 2. Synthesis of **CSP 3** triterpenoid brush-type phase.

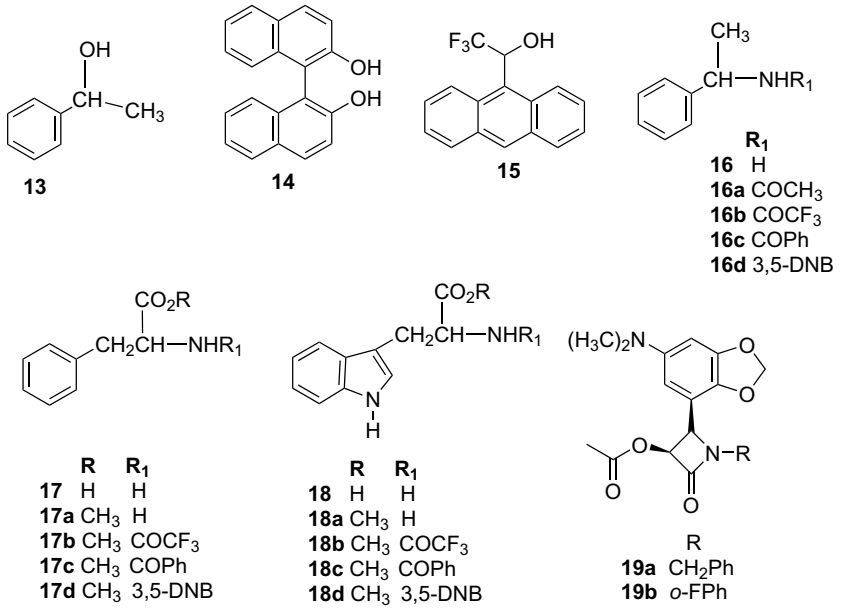

Chart 1.

CSP 1 and **CSP 2** were prepared from precursors **1** and **2**, respectively, as outlined in Figure 1. The carboxylic groups of **1** and **2**, directly bound to the stereogenic centre, were previously transformed into their acid chlorides **4** and **7**. Subsequently, intermediates **4** and **7** were reacted with the 10-undecenylamine spacer to afford the amides **5** and **8** in 93% and 86% yields, respectively. This derivatisation introduces a double bond, which is well known to be an appropriate structural moiety for the anchoring of chiral selectors to a silica gel support. In fact, hydrosilylation of amides **5** and **8** with dimethylchlorosilane in the presence of a catalytic amount of chloroplatinic acid quantitatively afforded monochlorosilane compounds **6** and **9**, respectively. Subsequently, these intermediates were covalently linked to a 5 μm porous silica gel via a straight nucleophilic reaction leading to **CSP 1** and **CSP 2**, respectively.

The complete synthesis of **CSP 3** is depicted in Figure 2. In order to prepare this triterpenoid phase, friedelin **3**, isolated from cork smoker wash solids, was selectively reduced to friedelan-3α-ol **3a**.[29] The friedelane scaffold does not contain suitable functionalities for enantioselective discrimination, such as π–π interactions; thus the hydroxyl group of **3a** was reacted with terephthaloyl chloride in the presence of 4-DMAP leading to the formation of derivative **10**. This intermediate now incorporates one aromatic moiety with potential binding properties and one free acyl group, which can be used to bind the spacer. Treatment of this intermediate with 10-undecenylamine gave the *N*-10″-undecenylamide compound **11**, which was hydrosilylated to silyl compound **12**, using the reaction conditions described for the preparation of the other two CSPs. Finally, this intermediate was directly linked to 5 μm silica gel support.

The grafting yield of the selector immobilised on the silica gel support was determined from the elemental analyses of either carbon or nitrogen (see Experimental). The results found are consistent with covalent linkage of the three selectors to the silica gel support and comparable with those reported for other brush-type phases. **CSP 2** shows a slightly higher grafting yield (0.31 mmol g^{-1}) than **CSP 1** and **CSP 3**.[32]

The three phases were then packed into 150 and 100 × 4.6 mm ID stainless-steel HPLC columns. In order to increase the enantioselectivity, endcapping of the modified silicas was carried out in situ throughout the reaction of the free silanol groups with hexamethyldisilazane.[33]

2.2. Evaluation of chiral resolution ability of the stationary phases

Selectors **1** and **2** have rigid diterpenoid architectures containing an aromatic moiety capable of enantioselective recognition of the aromatic analytes through π–π interactions. However, these two chiral molecules display different electronic binding properties, **2** with two electron-withdrawing nitro groups has a π acidic character, while **1** exhibits a π-basic character. In addition, **2** can establish enantioselective N-O···H hydrogen bonding interactions between the NO_2 groups and O–H or N–H groups from the analytes (Fig. 1). Therefore, both compounds seem very attractive candidates to be chiral selectors of novel brush-type phases. **CSP 3** has an extended pre-organised triterpenoid backbone coupled with an aromatic moiety via an ester group, which can be used concomitantly for enantioselective binding of the analytes. Moreover, the *N*-undecenylamide fragment of the CSPs provides N–H and CO binding groups, which extend the enantioselective discrimination possibilities via multiple and cooperative intermolecular hydrogen bonding interactions.

The enantioselective resolution capabilities of **CSP 1**, **CSP 2** and **CSP 3** were evaluated with four representative sets of chiral aromatic analytes composed of alcohols **13**–**15**, amines **16**–**d**, amino acid derivatives from phenylalanine **17**–**d** and tryptophan **18**–**d** and *cis*-β-lactams **19a**–**b**, respectively (Chart 1). All compounds were eluted as racemic mixtures under normal phase conditions. The two enantiomeric forms of alcohols **14** and **15** and amino acids **17** and **18** were also eluted separately in order to identify the elution order. For comparison, all compounds were also eluted on the (*R*,*R*)-Whelk-O1 commercial phase, which has been widely used for the separation of the enantiomers of a variety of compounds.[34] The chromatographic results are summarised in Table 1 together with the most adequate mobile phases compositions found.

CSP **1** is unable to promote the resolution of the racemic mixtures alcohols **13**–**15**, in spite of the several mobile phases with different degrees of polarity have been experimented.

α-methylbenzyl alcohol **13** exhibits a good resolution on **CSP 2** and **CSP 3** and (*R*,*R*)-Whelk-O1 with α values of 1.26, 1.43 and 1.68, respectively. The enantiomers of 9-anthryltrifluoromethylcarbinol **15** are separated onto **CSP 3** with an α of 1.23 while on the (*R*,*R*)-Whelk-O1 phase they are discriminated with a α value of only 1.16. The binding interactions between the (*S*)-**15** analyte and the selectors of **CSP 2** and **CSP 3** are stronger than those with the (*R*)-**15** analyte, as the latter is the first to be eluted from both columns. Whereas, the (*S*)-**15** analyte is the first to be eluted on the (*R*,*R*)-Whelk-O1 phase.

An efficient enantioseparation of 1,1′-bi-2,2′-naphthol **14** was achieved on **CSP 2** phase with an α value of 1.14. This result is noteworthy compared to a resolution of 1.04 obtained with the commercial phase for this atropisomer. In fact, the separation of binaphthol compounds by (*R*,*R*)-Whelk-O1 phase is achieved only after derivatisation of the hydroxy groups of the atropisomer with a butane bridge.[35] Separation of **14** by **CSP 2** is probably due to the formation of transient complexes stabilised by enantioselective hydrogen bonds between the nitro groups from the π-acidic selector, and free hydroxy groups of analytes, which can be complemented concomitantly with π–π interactions between the π-acidic **CSP 2** and the π-basic binaphthol aromatic sites. These interactions are more effective with the (*S*)-analyte. Moreover, it is interesting to note that the best enantioseparations of alcohols **13**–**15** on this phase were achieved using a low polarity mobile phase composed of *n*-hexane/propan-2-ol/trifluoracetic acid (99:1:0.09 v/v), in which the acid was added in order to improve the peak shapes.

The chromatographic data shows that the (*R*,*R*)-Whelk-O1 is the more appropriate to separate the majority of amine derivatives than the brush-type phases described here, with the exception of the underivatised amine **16**, which is well separated by **CSP 3** with an α of 1.55. This racemate is not resolved by a commercial phase. Amine derivative **16b** with a trifluoracetyl group is also well resolved upon **CSP 3** with an α of 1.74, but the enantiochromatographic separation of this compound on (*R*,*R*)-Whelk-O1 phase occurs with α 3.00. The *N*-3,5-dinitrobenzoyl (*N*-3,5-DNB) amine derivative **16d** with a π-acidic character is slightly discriminated on **CSP 1** with an α of 1.04 and **CSP 2** with an α of 1.07. This compound finds an efficient resolution on (*R*,*R*)-Whelk-O1 phase with an α of 1.98.

Table 1. Chromatographic resolution of racemic compounds on **CSP 1**, **CSP 2**, **CSP 3** and commercial (*R*,*R*)-Whelk-01

Compound	CSP 1			CSP 2			CSP 3			(*R*,*R*)-Whelk-01		
	α	k'_1	R_s	α	k'_1	R_s	α	k'_1	R_s	α	k'_1	R_s
13	1.00	—		1.26[a]	0.66	1.13	1.43[b]	0.45	2.00	1.68[c]	0.69	3.50
14	1.00	—		1.14[a]	10.47[n]	1.54	1.00	—	—	1.04[d]	6.57[o]	—
15	1.00	—		1.08[a]	9.95[n]	0.65	1.23[e]	1.26[n]	0.80	1.16[e]	1.89[o]	1.13
16	1.00	—	—	1.00	—	—	1.55[j]	0.20	2.00	1.00	—	—
16a	1.00			1.00	—	—	1.00	—	—	2.21[c]	3.30	3.91
16b	1.06[f]	4.55	0.70	1.06[h]	3.62		1.74[k]	0.28	—	3.00[e]	1.64	8.82
16c	1.00	—	—	1.09[h]	14.0	0.76	1.00	—	—	3.20[c]	3.60	9.40
16d	1.04[g]	22.36	—	1.07[h]	17.8	0.82	1.00	—	—	1.98[c]	7.20	4.85
17	1.00	—	—	1.00	—	—	1.00	—	—	1.00	—	—
17a	4.83[d]	0.70[n]	3.79	2.87[i]	1.62[n]	1.13	2.44[e]	0.35[n]	3.40	1.00	—	—
17b	1.30[c]	0.92[o]	0.89	1.05[c]	1.21[n]	—	1.00	—	—	1.00	—	—
17c	1.04[e]	2.58	—	1.00	—	—	1.00	—	—	1.00	—	—
17d	3.65[e]	0.92[o]	6.40	5.03[e]	1.03[n]	9.22	2.94[c]	0.32[o]	1.56	1.30[l]	1.42[o]	—
18	1.00			1.00	—	—	1.00	—	—	1.00		
18a	2.00[d]	0.73[n]	1.95	1.00	—	—	1.00	—	—	1.00		
18b	1.00	—	—	1.00	—	—	1.00	—	—	1.00		
18c	1.00	—	—	1.34[e]	8.68[o]	1.69	1.00	—	—	1.00		
18d	1.00	—	—	1.00	—	—	1.00	—	—	1.15[l]	1.23[o]	—
19a	3.94[e]	0.16	6.78	1.00	—	—	1.00	—	—	1.36[m]	4.00	3.35
19b	2.93[e]	0.17	4.78	1.00	—	—	1.00	—	—	1.41[m]	4.20	3.45

Mobile phase: [a]*n*-hexane/propan-2-ol/trifluoroacetic acid (99:1:0.09) (v/v); [b]*n*-hexane/dichloromethane (80:20); [c]*n*-hexane/propan-2-ol (90:10); [d]*n*-hexane/propan-2-ol (80:20); [e]*n*-hexane/propan-2-ol (95:5); [f]*n*-hexane/propan-2-ol (99:1); [g]*n*-hexane/propan-2-ol/trifluoroacetic acid (97:3:0.09); [h]*n*-hexane/propan-2-ol/methanol (96:3.5:0.5); [i]*n*-hexane/propan-2-ol/ethanol (99:0.5:0.5); [j]*n*-hexane/dichloromethane (90:10); [k]*n*-hexane/dichloromethane (95:5); [l]*n*-hexane/propan-2-ol/ethanol (95:2:3); [m]*n*-hexane/propan-2-ol (50:50); [n](*R*) absolute configuration of the first eluted enantiomer; [o](*S*) absolute configuration of the first eluted enantiomer.

The free amino acid **17** is not separated by any of the four phases either. In contrast, the methyl ester of phenylalanine **17a** has a good resolution on the three novel phases with enantioseparation factors of 4.83, 2.87 and 2.44 for **CSP 1**, **CSP 2** and **CSP 3**, respectively; while on the commercial phase, the racemate of this derivative is not separated. This result suggest that the presence of a methyl ester can improve enantioseparation as reported previously by several authors.[36] However, the attachment of bulky substituents at the amine group, such as *N*-trifluoracetyl in **17b** and *N*-benzoyl (an extra π-donor aromatic binding site) in **17c**, decreases the enantiodiscriminating capability of all the brush-type phases. Indeed, only racemate **17b** is separated on **CSP 1** with an α of 1.30 while **17c** is only slightly resolved with an α of 1.04 when the polarity of the mobile phase is reduced (see Table 1). These results indicate that the steric bulk of the *N*-substituent prevents the formation of enantioselective N–H···O hydrogen bonds between the analytes and the selectors. Efficient enantioselective separations of the analytes of the *N*-3,5-dinitrobenzoyl (3,5-DNB) methyl ester amino acid derivative **17d** are obtained on **CSP 1**, **CSP 2** and **CSP 3** with separation factors of 3.65, 5.03 and 2.94, respectively. It is noteworthy that the best enantioseparation of this π-acidic analyte is achieved with the π-acidic **CSP 2** phase suggesting that the formation of the transient complexes is mainly governed by enantioselective hydrogen bonding interactions rather than π–π interactions. We will return to this point later. The racemate of **17d** is also resolved by the commercial phase, but with a lower α of 1.30.

The enantioseparation results for tryptophan amino acid **18** and their ester derivatives **18a**–**d**, by comparison with those obtained for phenylalanine suggest that the presence of an indolic ring decreases or turns off the enantioselectivity. Indeed, methyl ester **18a** is resolved upon **CSP 1** with an α of 2.00, while the analytes of methyl ester **18c** having a *N*-benzoyl group are separated by **CSP 2** with an α value of 1.34. The *N*-(3,5-DNB) methyl ester derivative **18d** is not discriminated by any of the three **CSPs**. This derivative is resolved on the (*R*,*R*)-Whelk-O1 phase with an α of 1.15. Furthermore, **CSP 3** was shown to be inadequate in resolving any of the tryptophan amino acid derivatives.

The two *cis*-β-lactams display low capacity factors, below 0.7, but they are resolved by **CSP 1** with α values of 3.94 for **19a** and 2.93 for **19b**. By contrast, these compounds are more retained on the (*R*,*R*)-Whelk-O1 phase with k'_1 values of 4.00 for **19a** and 4.20 for **19b**, nevertheless its separation on this phase is less efficient with α values of 1.36 and 1.41 for **19a** and **19b**, respectively.

2.3. Molecular modelling studies

In order to obtain further insights into the enantioselective binding behaviour of **CSP 1** and **CSP 2** phases, molecular mechanics energy calculations were carried out for the diastereomeric complexes between the selectors of these two chiral stationary phases and the two enantiomers amino acid derivatives **17a** and **17d**, which exhibit the higher separation factors on both phases (see Table 1). The starting geometries of all the binary complexes were generated using the docking strategy described in Section 4.

Figure 3 shows the structures of the lowest energy binding associations found for each diastereomeric complex with the corresponding differences in molecular mechanics energies between (*R*)- and (*S*)-complexes (Δ_{R-S}). The binding

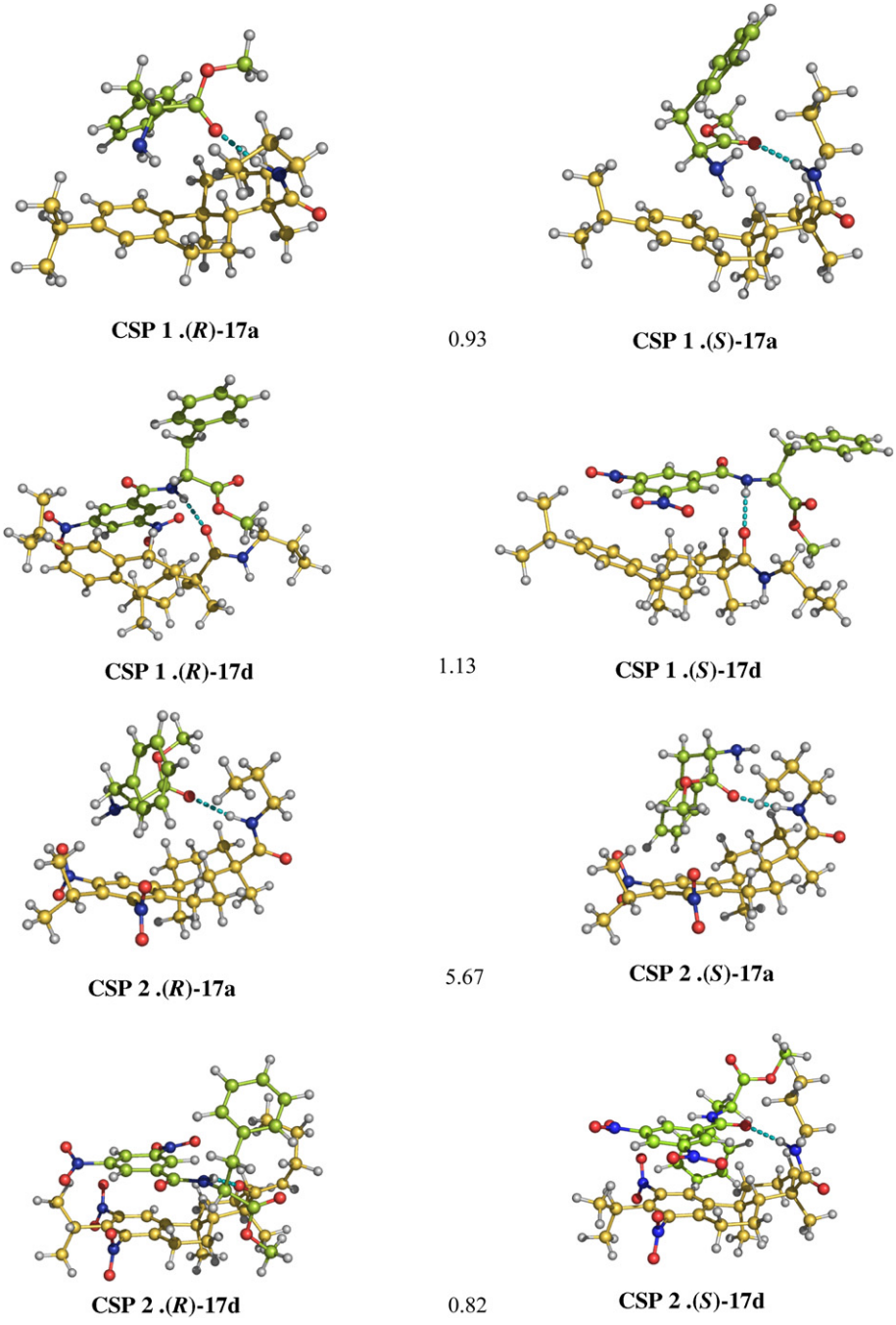

Figure 3. Lowest energy binding scenarios found on conformational analyses on diastereomeric complexes with Δ_{R-S} energies (see text) in kcal mol^{-1}. The carbon skeleton of selectors and analytes are in yellow and green, respectively. The oxygen and nitrogen atoms are in the conventional colours red and blue, respectively. The hydrogen bonding interactions between the binding sites are drawn as dotted lines in light blue.

regions of the **CSP 1** phase are illustrated in Figure 4 through the isodensity contour map, which was drawn sampling all (*R*)-analyte orientations from the minimised **CPS 1·17a** binding scenarios saved along the molecular dynamics quenching run. The shell surface almost encases the selector domain validating the docking strategy adopted. As would be expected, the most densely populated region is the hydrogen bonding site of **CSP 1**, namely the amide group. Subsequently, MD simulations of 40 ns were carried out in the gas phase at 300 K using the lowest energy structures shown in Figure 3 as starting models.

The binding energy (ΔE) associated with an enantioselective interaction between the selector and a single enantiomer is calculated using the equation:

$$\Delta E = E_{\text{complex}} - E_{\text{selector}} - E_{\text{enantiomer}} \quad (1)$$

In which E_{complex} is the total energy for the diastereomeric complex while E_{selector} and $E_{\text{enantiomer}}$ are the individual energies for the selector and the enantiomer, respectively. Usually, these three energetic terms are evaluated from three independent simulations carried with complex, selector and the analyte, respectively. However, when the

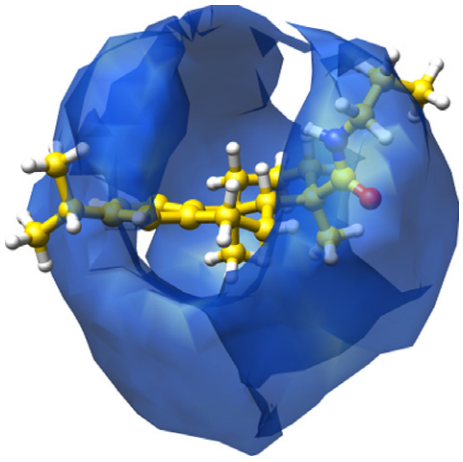

Figure 4. Isodensity contour map for **CSP 1**·(***R***)-**19a** built sampling all (*R*)-**19a** analyte orientations saved over molecular dynamics run in the gas phase.

formation of the transient complexes occur without a significant conformational change of selector and analytes, these three individual energetic contributions can be evaluated from the MD simulation of the complex and then the binding energy is only determined by electrostatic (ΔE_{elec}) and van der Waals (ΔE_{vdw}) energy differences being Eq. 1 simplified to

$$\Delta E = \Delta E_{elec} + \Delta E_{vdw} \quad (2)$$

The ΔE_{elec} and ΔE_{vdw} terms are average energy differences calculated with snapshots of the complex, selector and analyte retrieved by post-processing the MD trajectory file of each diastereomeric complex with the MM-PBSA method[37] as described in Section 4. The results obtained for the eight complex diastereomers studied are compiled in Table 2. The evolution of accumulated binding energies for 40 ns of simulation is plotted in Figure 5 for the transient complexes between the analytes of **17a** and **17d** and the **CSP 1** selector and in Figure 6 for the complexes formed with these analytes and the **CSP 2** selector. The plot for the two **CSP 1**·**17a** diastereomeric associations (Fig. 5a) shows that after the first 5 ns of simulation the (*S*) enantiomer is more tightly bound to the phase and the interaction energy of the two diastereomeric complexes remains almost constant until the end of the simulations. Thus, the (*R*) enantiomer is predicted to be the first one to be eluted from the HPLC column, which is in agreement with experimental findings. Figure 5b shows that over the majority of the simulation, the **CSP 1** selector has a clear binding preference for the (*R*) enantiomer of **17d**. The (*R*) diastereomeric complex displays a constant energetic stabilisation from 3 ns until the end of the simulation. By contrast, the simulation with the (*S*) complex starts with a marked increase of the binding energy of simulation until 16 ns of simulation, then the energy shows a progressive slight decrease for the remaining 24 ns of simulation apart from a short period of 2 ns around 26 ns.

Table 2. Interaction energies (kcal mol^{-1}) for the diastereomeric complexes with **CSP 1** and **CSP 2** selectors averaged over the 200,000 frames taken from the 40 ns molecular dynamics simulation in the gas phase

Phase	Analyte	ΔE_{ele}	ΔE_{vdw}	ΔE	$\Delta\Delta E_{ele}$[a]	$\Delta\Delta E_{vdw}$[b]	$\Delta\Delta E$[c]
CSP 1	(***R***)-**17a**	−3.95	−8.63	−12.58	0.36	0.14	0.50
	(***S***)-**17a**	−4.31	−8.77	−13.08			
	(***R***)-**17d**	−10.37	−16.47	−26.84	−1.30	−1.18	−2.48
	(***S***)-**17d**	−9.07	−15.29	−24.36			
CSP 2	(***R***)-**17a**	−4.40	−10.29	−14.69	0.53	0.04	0.57
	(***S***)-**17a**	−4.93	−10.33	−15.26			
	(***R***)-**17d**	−7.74	−17.51	−25.25	1.00	−0.20	0.80
	(***S***)-**17d**	−8.74	−17.31	−26.05			

[a] $\Delta\Delta E_{ele} = \Delta E_{ele}(R) - E_{ele}(S)$.
[b] $\Delta\Delta E_{vdw} = \Delta E_{vdw}(R) - E_{vdw}(S)$.
[c] $\Delta\Delta E = \Delta E(R) - \Delta E(S)$. Remaining energy terms are defined in the text.

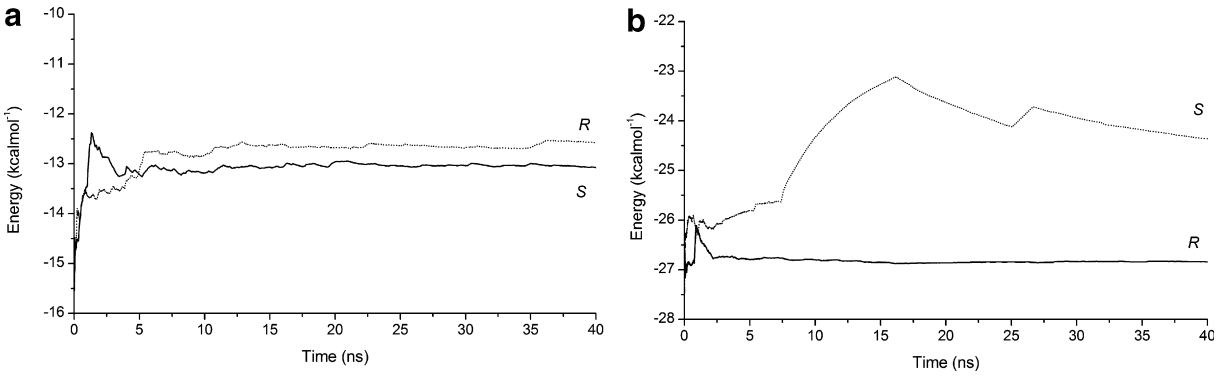

Figure 5. Evolution of the average binding energies over the MD simulations on diastereomeric binding associations between **CSP 1** and analytes **17a** (a) and **17d** (b).

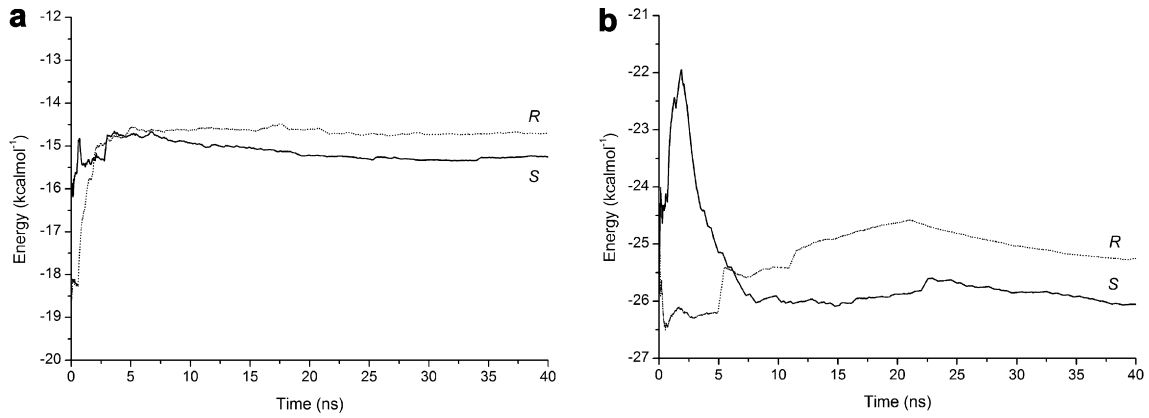

Figure 6. Evolution of the average binding energies over the MD simulations on diastereomeric binding associations between **CSP 2** and analytes **17a** (a) and **17d** (b).

Figure 6a shows that the simulation between the (*R*)-**17a** and the **CSP 2** selector starts with a pronounced increase of the average binding interaction energy and during the first 3 ns of the MD the enantioselective binding forces favour the formation of **CSP 2**·(***R***)-**17a** complex. However, after 5 ns, this binding preference is reversed with the binding energies for the two diastereomeric complexes remaining almost constant to the end of the MD simulations.

The graphs for **CSP 2**·**17d** diastereomeric complexes plotted in Figure 6b show that the binding interaction with the (*S*) enantiomer is favoured after the first 5.5 ns until the end of the simulation, which agrees with the experimental chromatographic data. Further insight on the enantioselective discrimination is derived from the difference between the intermolecular binding energies of (*R*) and (*S*) complexes, $\Delta\Delta E = \Delta E_R - \Delta E_S$, which can be considered to be a quantitative measure of the chiral discrimination. The $\Delta\Delta E$ values calculated for all pairs of diastereomeric complexes, given in Table 2, are in agreement with the experimental HPLC elution orders found for the (*R*) and (*S*) analytes of **17a** and **17d** on **CSP 1** and **CSP 2**. The negative values of ΔE_{elec} and ΔE_{vdw} energy differences obtained for each diastereomeric complex indicate that in all of them both terms contribute to hold the receptor and the analyte together. Furthermore, the van der Waals interactions are the dominant stabilising intermolecular forces while the electrostatic binding interactions are the discriminating forces responsible for the $\Delta\Delta E$ energy differences between the (*R*) and (*S*) complexes. The unique exception is the enantioselective binding of the **CSP 1** to the analytes of **17d**, where the energy differences between (*R*) and (*S*) complexes are -1.30 kcal mol^{-1} for $\Delta\Delta E_{\text{elec}}$ term and -1.18 kcal mol^{-1} for the $\Delta\Delta E_{\text{vdw}}$ term leading to a $\Delta\Delta E$ discriminating energy of -2.48 kcal mol^{-1}. Furthermore, these enantiodifferentiating energies ($\Delta\Delta E$) are very small when compared with the energies associated with the formation of each diastereomeric complex (ΔE). The $|\Delta\Delta E|$ values lead to the following resolution orders for (*R*) over (*S*) **17d** > **17a** on **CSP 1** and **CSP 2**. The order for **CSP2** is entirely consistent with experimental α values while the order for **CSP 1** is not. However, this result is not necessarily inconsistent with our results since the $\Delta\Delta E$ term represents the molecular mechanics energy, which is only one of the three components of the free energy. The remaining two, the entropic and the enthalpic contributions were not taken into account in our calculations nor were the solvent effects. However, the entropy was estimated for all diastereomeric pairs using the NMODE program as implemented in AMBER 8 package. The values for the (*R*) and (*S*) complexes were similar showing that entropy contribution is negligible on the chromatographic chiral discrimination as suggested previously by Lipkowitz.[38] Finally, the molecular modelling models are an oversimplification of the chromatographic experiments since that neither the spacers nor the anchor of the spacer onto the silica gel support are taken into account.

Further analysis of MD simulations was carried out with the ANAL program within the AMBER 8 package. The selectors of the **CSP 1** and **CSP 2** phases were split at chiral carbon C-4 into three fragments as shown in Figure 7. The first fragment is the *N*-propyl amide group, the second is the diterpenoid backbone and the methyl group is the third one. This fragment decomposition is arbitrary, albeit it provides a better understanding of how the enantiomers are discriminated. The energies associated with each one of these three fragments interacting with the analytes are collected in Table 3.

The selectors and analyte are held together by short-range dispersion forces and so the diterpenoid fragment is mainly responsible for the stabilisation of most of the diastereomeric complexes. The second most important stabilising factor comes from the amide group, which interacts with the analytes via electrostatic forces. As mentioned above, the unique exception is the complex between **CSP 1** and the (*R*) enantiomer of **17d**, where both fragments contribute almost identically towards stabilisation. The methyl group favours only marginally the formation of the complexes because the approach of the analytes to the chiral binding site of **CSP 1** and **CSP 2** from the side of the methyl group is not favoured because of steric repulsions. The enantioselective differentiating forces (electrostatic interactions as reported above) are consistent with the pattern of the hydrogen bonds established by the selector and

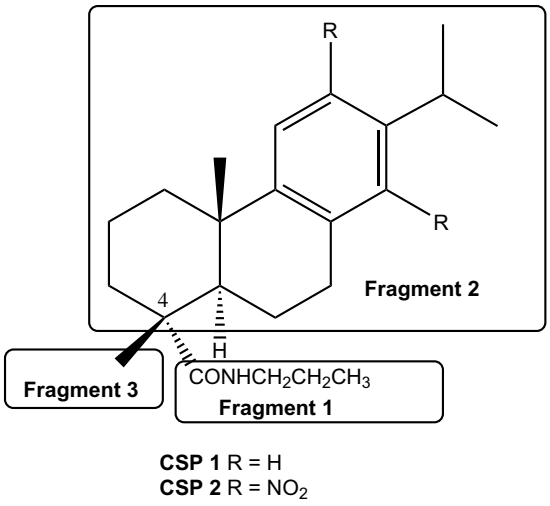

Figure 7. Diagram showing the fragment decomposition of **CSP 1** and **CSP 2** selectors used on energetic analyses.

the analytes during the molecular simulations. Table 4 lists the dimensions of the hydrogen bonds found for all transient complexes with occupancies greater than 10% and an H···A distance less than 2.50 Å, A being an acceptor atom. The **CSP 1** and **CSP 2** phases discriminate the analytes of **17a** and **17d** diastereomers mainly through the N–H···O=C hydrogen bonding interactions established between the N–H and carbonyl binding sites from the amide group of the phase and analyte, respectively. This interaction was found to be quite strong in all diastereomeric complexes with average H···O distances within the narrow range of 2.09–2.26 Å. Furthermore, this discrimination comes mainly from the different occupancies (the percentage of time that the hydrogen bond is formed over the complete MD trajectory) of this hydrogen for the *R* and *S* complexes. For example, the N–H···O=C hydrogen participates with an occupancy of 99.3% for the formation of **CSP 1**·(***R***)**-17d** and only with 77% for **CSP 1**·(***S***)**-17d** and the formation of the first complex is favoured by an electrostatic stabilisation of 1.30 kcal mol^{-1} in the gas phase. Surprisingly, the nitro groups of **CSP 2** occasionally establish weak N–H···O hydrogen bonds with the N–H binding site of the *R* analyte but not with the *S* isomer. However this will have a marginal impact on enantioresolution.

As reported above **CSP 1** was found experimentally to be unable to discriminate between the **17a** analytes in *n*-hexane but could discriminate with a mobile phase composed of *n*-hexane and propan-2-ol (ratio 80:20). In order to eval-

Table 3. Energetic contribution of two fragments in the binding interaction between the analytes and **CSP 1** and **CSP 2** phases

		Fragment 1			Fragment 2			Fragment 3[a]		
	Analyte	ΔE_{ele}	ΔE_{vdw}	ΔE_{total}	ΔE_{elec}	ΔE_{vdw}	ΔE_{total}	ΔE_{elec}	ΔE_{vdw}	ΔE_{total}
CSP 1	(***R***)**-17a**	−3.11	−2.23	−5.34	−0.82	−6.26	−7.08	−0.02	−0.13	−0.15
	(***S***)**-17a**	−3.36	−2.43	−5.79	−0.94	−6.21	−7.15	−0.02	−0.12	−0.14
	(***R***)**-17d**	−10.32	−3.41	−13.73	−0.16	−12.77	−12.93	0.12	−0.29	−0.17
	(***S***)**-17d**	−7.05	−3.25	−10.30	−2.08	−11.74	−13.82	0.06	−0.28	−0.22
CSP 2	(***R***)**-17a**	3.69	−2.80	0.89	−7.93	−7.41	−15.34	−0.16	−0.08	−0.24
	(***S***)**-17a**	4.35	−2.51	1.84	−9.29	−7.71	−17.00	−0.17	−0.09	−0.26
	(***R***)**-17d**	−7.51	−3.32	−10.83	−0.26	−13.92	−14.18	0.03	−0.27	−0.24
	(***S***)**-17d**	−8.72	−3.27	−11.99	−0.15	−13.70	−13.85	0.11	−0.32	−0.21

Values are averaged from the 200,000 frames taken from the 40 ns molecular dynamics simulation in the gas phase.
[a] The fragment definitions are given in the text and in Figure 7.

Table 4. Average dimensions of the hydrogen bonds in transient diastereomeric complexes formed by selectors (*S*) and enantiomers (*E*)

Complex	Selector	Enantiomer	% Occupation	H···A (Å)	D–H···A (°)
CSP 1·(***S***)**-17a**	N–H	O=C	71.9	2.21(26)	163(8)
CSP 1·(***R***)**-17a**	N–H	O=C	64.7	2.25(28)	161(9)
CSP 1·(***S***)**-17d**	O=C	N–H	77.0	2.11(24)	154(10)
	H–N	O=C	20.0	2.30(27)	158(9)
CSP 1·(***R***)**-17d**	O=C	N–H	99.3	2.09(22)	158(10)
CSP 2·(***S***)**-17a**	N–H	O=C	80.4	2.22(27)	165(9)
CSP 2·(***R***)**-17a**	N–H	O=C	64.6	2.26(28)	163(9)
	N–H	N	14.1	2.43(29)	159(12)
	NO_2	NH_2	11.6	2.47(31)	151(17)
CSP 2·(***R***)**-17d**	O=C	N–H	72.8	2.10(23)	159(10)
	N–H	O=C	22.5	2.24(26)	164(8)
CSP 2·(***S***)**-17d**	O=C	N–H	93.6	2.11(23)	156(12)

O=C and N–H denote oxygen and hydrogen atoms from the amide binding site; O and O–H denote oxygen and hydrogen atoms from the alcohol binding site, N and NH_2 denote nitrogen and hydrogen atoms from amine group; NO_2 denote oxygen atoms from the NO_2 group. A and D represent acceptor and donor atoms, respectively.

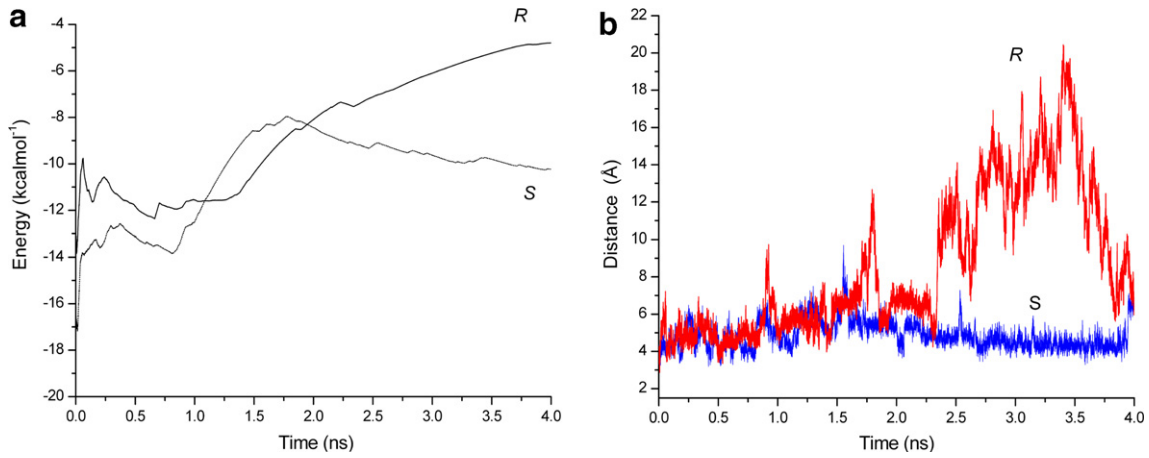

Figure 8. Molecular dynamics simulations of the enantioselective binding recognition of **19a** analytes by **CSP 1** in the *n*-hexane/2-propan-ol (80:20 vv) mobile phase: (a) evolution of the cumulative average binding energies; (b) variations of the intermolecular distance between the centre of mass of aromatic rings of the selector and (***R***)-**17a** and (***S***)-**17a** analytes.

uate the role of the polarity of the mobile phase on the enantioresolution of **17a** enantiomers by **CSP 1**, molecular dynamics simulations in this medium were carried out for 4 ns. The binding energy difference $\Delta\Delta E$ between the (*R*) and (*S*) analytes, calculated with the MM-PBSA method[37] is 5.43 kcal mol^{-1}, showing a significant increase compared to the value of 0.50 kcal mol^{-1} determined in the gas phase. The van der Waals and the electrostatic energy components are both attractive contributing to the stabilisation of the two diastereomeric complexes. However, the formation of the (*S*) complex is favoured by 2.10 and 3.32 kcal mol^{-1}, respectively. The average accumulated binding intermolecular energies for the two diastereomeric complexes are plotted against time in Figure 8a, while Figure 8b shows the variation in intermolecular distances between the centres of mass of the selector and the analytes. During the

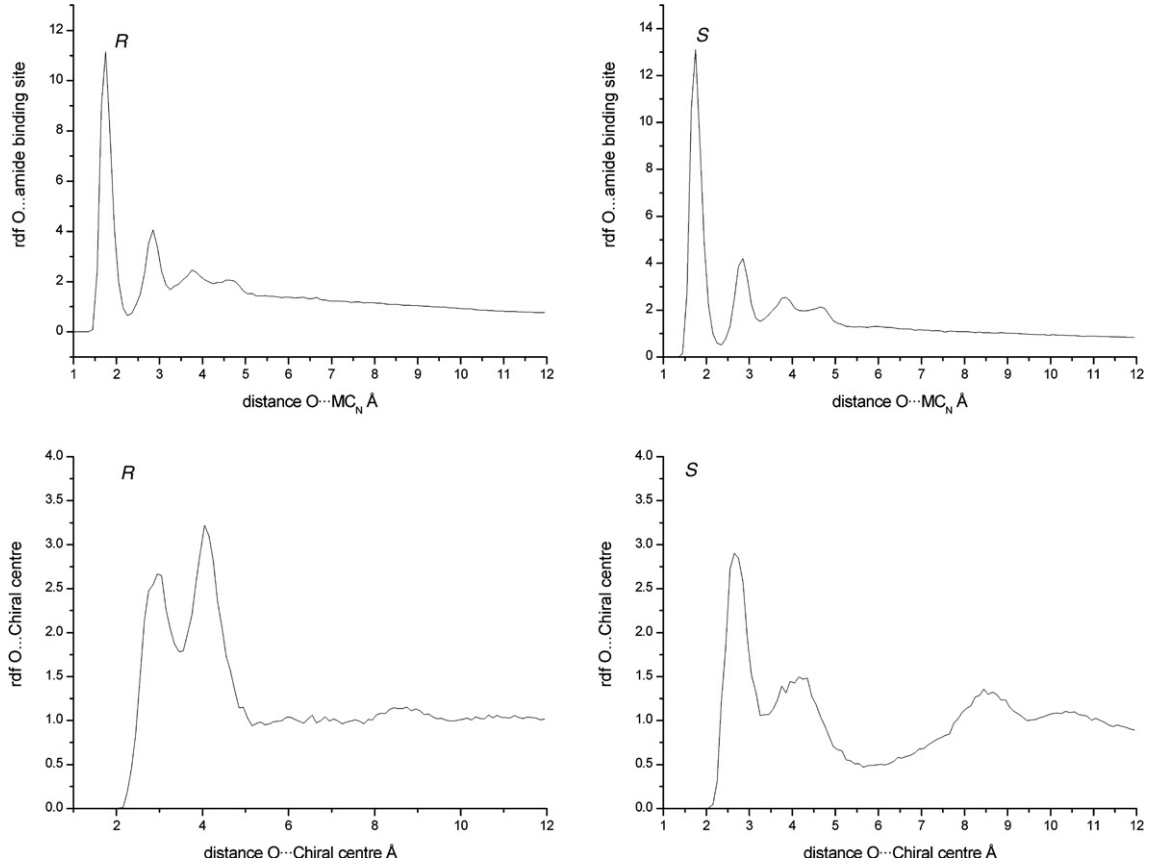

Figure 9. Rdfs showing the interaction between the propan-2-ol solvents molecules with (*R*) and (*S*) **CSP 1**·**17a** diastereomeric complexes: top with the **CSP 1** selector; bottom with the **17a** analytes. MC_N represents the centre of mass of the amide binding group of the selector.

simulation the selector binds tightly with the (*S*) analyte such that this intermolecular distance displays only small changes around its average value of ca. 4.0 Å. By contrast, for the (*R*) analyte the binding association is interrupted during two periods of simulation, between 1.6 and 1.8 ns and 2.3–3.8 ns, with concomitant solvation of the analyte with propan-2-ol eventually via weak N–H···O–H hydrogen bonding interactions with H···O distances ranging from 2.26 to 2.38 Å. At this stage, it is important to note that in order to evaluate the solvent discriminating role, that is the competition between the propan-2-ol solvent molecules and the analytes for the binding sites of phase, no restraint distance was applied between the enantiomers and the selector. The binding energy for **CSP 1**·(***S***)-**17a** is lower than that found for **CSP 1**·(***R***)-**17a** over the time of simulation, with the exception for the period between 1.2 and 1.8 ns. The fragment decomposition analysis indicates that in solution discriminating energies are derived from the binding interaction between the amide group and the diterpenoid moiety with the analytes. As found in the gas phase calculations, **CSP 1** binds with the analytes via N–H···O=C hydrogen bonds with occupancies of 26% and 61% for (*R*) and (*S*) analytes, respectively, which is consistent with an electrostatic stabilisation of the (*S*) complex by 1.51 kcal mol^{-1}. The diterpenoid fragment interacts with analytes via dispersive van der Waals forces, which also favour the formation of the latter complex in 2.51 kcal mol^{-1}. The radial distribution functions (rdf) for the intermolecular distances from the oxygen of the propan-2-ol solvent molecules to the chiral centre of analyte and the centre of mass of the amide binding group are presented in Figure 9 for the two **CSP 1**·(***S***)-**17a** and **CSP 1**·(***R***)-**17a** diastereomeric complexes and show identical profiles with two well-defined peaks centred at 1.9 and 3.0 Å. The first one has higher intensity characteristic of O–H···O=C hydrogen bonding interactions between propan-2-ol molecules and the carbonyl from the **CSP 1**. Indeed, this peak integrates approximately to 3.95 for (*R*) complex and 4.53 for (*S*) complex, suggesting that in this diastereomeric binding association the selector is more accessible for solvent hydrogen bonding interactions. On the other hand, the rdfs for the interaction with analytes show two broad peaks consistent with the formation of two solvent shells at ca 3.2 and 4.5 Å around the analyte (*R*) while for the (*S*) analyte only the first coordination shell is observed. Therefore, propan-2-ol molecules solvate better with the (*R*) analyte than the (*S*) analyte leading to the enantioselective separation of **17a** analytes on **CSP 1**.

3. Conclusions

Three novel brush phases based on two terpenoid skeletons with different enantioselective capabilities were prepared. The **CSP 3** phase can resolve racemates of alcohols, specifically derivatives containing fluorine substituents, and free amines. **CSP 2** is the only phase to resolve unequivocally 1,1′-binaphthol atropisomers. This result is noteworthy since that with the brush-type phases reported in the literature, the enantioseparation of these alcohols is achieved only with their derivatives. Good enantioseparations of *cis*-β-lactams and *N*-benzoyl tryptophan amino acid derivatives were achieved on **CSP 1**. All three phases can be also used for the efficient resolution of racemates of *N*-trifluoracetyl and *N*-3,5-DNB ester phenylalanine derivatives. Experimental results show that **CSP 2** containing two nitro groups can discriminate better than **CSP 1**. Therefore, the introduction of the two nitro groups at the C-12 and C-14 positions of the aromatic ring of the dehydroabietic acid provides new and additional sites for intermolecular interactions with chiral analytes and this can significantly enhance chiral recognition ability, especially for binaphthols and methyl ester phenylalanine derivatives. The highest α value was found for the enantioresolution of **17d** upon **CSP 2**. In this case, the phase and selector both have π-acidic character showing that the cooperative binding interaction between π-acidic and π-basic centres is not necessary for the success of an enantioseparation. Indeed, our molecular modelling studies shown that the stability of the transient complexes formed between **CSP 1** and **CSP 2** and analytes **17a**, **17d** and **14** is determined by van der Waals interactions while the enantioselectivity is mainly dictated by hydrogen bonds. Moreover, the efficiency of enantioseparation depends largely on the expertise of the analytical chemist to discover a mobile phase with an appropriate polarity as shown by our experimental and simulations studies in an *n*-hexane/propan-2-ol solvent mixture. The chromatographic data obtained for the four different families of compounds composed of a representative number of structurally related molecules also shows that the molecular design of chiral phases for general use, even for similar compounds, is still a hard task and a challenge for the chemists as recently noticed.[39] The ability of **CSP 1**, **CSP 2** and **CSP 3** phases to promote the chiral enantioseparation of the aminoacid derivatives using reverse polarity mobile phases such as water and methanol are in progress in our laboratories.

4. Experimental

4.1. Chemicals and reagents

12,14-Dinitrodehydroabietic acid **2** was synthesised by the nitration of dehydroabietic acid **1**,[31] which was isolated from commercially dehydrogenated rosin.[28] Friedelin **3** was isolated from cork smoker wash solids while the friedelan-3α-ol derivative **3a** was prepared by the selective reduction of friedelin **3**.[29]

Toluene and THF were refluxed in the presence of sodium benzophenone and distilled before use. The remaining reagents and solvents were used without further purification. All chiral test compounds are drawn in Chart 1 together with the numbering scheme adopted. For amines, amino acids and *cis*-β-lactams the numbering scheme is composed of a number indicating the type of compound and a letter used to distinguish between molecules with different R and R_1 substituents. The chiral test compounds **14**–**18** were purchased from Aldrich or Merck. Racemic mixture of alcohol **13** was prepared by the reduction of the corresponding ketones with $LiAlH_4$. Amine **16a**–**c**, amino acid **17a**–**d** and **18a**–**d** derivatives were synthesised from their counterparts using standard procedures. Thus, the analytes

of methyl esters **17a** and **18a** were obtained by the treatment of the corresponding analytes of **17** and **18** with thionyl chloride in methanol. Reaction of **16** with acetic and trifluoroacetic anhydrides yielded the amide derivatives **16a** and **16b**, respectively, as racemic mixtures. Treatment of **16**, **17** and **18** with benzoyl chloride in the presence of pyridine in toluene afforded compounds **16c**, **17c** and **18c**, respectively; while derivatives **16d**, **17d** and **18d** were obtained using 3,5-dinitrobenzoyl chloride under the same reaction conditions. The *cis*-β-lactams **19a** and **19b** were synthesised following the synthetic procedure described in Ref. 40, and spectroscopic data recorded (comprise $[\alpha]_D$ for each analyte) for all derivatives are consistent with their structures. Silica gel for TLC refers to Merck silica gel GF254 and for flash chromatography to Merck silica gel 60 230–400 mesh. Organic phases were dried over anhydrous sodium sulfate.

Porous spherical silica gel Nucleosil® 100 Å–5 μm from Macherey-Nagel (Düren, Germany; Batch 20404134) was used as the support material of the three CSPs. Mobile phases were prepared using *n*-hexane and the organic modifiers methanol, propan-2-ol, ethanol and dichloromethane of HPLC-grade Riedel-deHaën (Germany).

Comparative chromatographic studies were carried out on the commercial column (*R*,*R*)-Whelk-O1 (LiChroCART® 250-4) purchased from the Merck Company.

4.2. Instrumentation

The chromatographic separations were performed using a Spectra-Physics liquid chromatograph system with a UV spectra Chrom 100 detector, injector equipped with a 20-μL sample loop, connected to a Chrom Jet register. The UV detector was operated at 254 nm. All separations were carried out at room temperature. The dead time (t_0) of the column was determined by the retention time of 1,3,5-tri-*tert*-butylbenzene, a presumed unretained analyte. The separation factor (α) between analytes and resolution factor (R_s) were defined as

$$a = \frac{t_2 - t_0}{t_1 - t_0} = \frac{k'_2}{k'_1} \quad (3)$$

$$R_s = \frac{2(t_2 - t_1)}{W_1 + W_2} \quad (4)$$

where t_1 and t_2 are the retention times, k'_1 and k'_2 are the capacity factors, W_1 and W_2 are the peak widths at the base for the first and second analytes to leave the column, respectively.

^{1}H and ^{13}C NMR spectra were recorded on a General Electric GE Plus-300 spectrometer. Chemical shifts were reported in parts per million (ppm) relative to tetramethylsilane as the internal standard. The following abbreviations were used: s = singlet; br s = broad singlet; d = doublet; br d = broad doublet; dd = double doublet; t = triplet; m = multiplet; coupling constants *J* are expressed in hertz (Hz). MS spectra were obtained on a Kratos MS-25 RF spectrometer via electron impact using an ionising energy of 70 eV or through fast atom bombardment (FAB) on a 3-nitrobenzyl-alcohol matrix. High-resolution MS spectra (HRMS) were obtained on a FTICR/MS Finnigan FT/MS 2001-DT spectrometer at 70 eV by electron impact or on a Finnigan MAT 900 ST spectrometer by ESI. Infrared (IR) spectra were recorded on a Perkin–Elmer 1725X FTIR spectrometer. Melting points were taken on a Reichert Thermovar thermal analyser and are uncorrected. Elemental analyses were performed in a CE EA-1110 microanalyser. Optical rotations were measured at the sodium D-line on a Perkin–Elmer 241 polarimeter.

4.3. Synthesis of CSP 1

CSP 1 and **CSP 2** phases were prepared by covalent link of **1** and **2** onto the silica gel support following similar synthetic procedures (Fig. 1).

4.3.1. 10-Undecenylamine spacer and its 10-undecenamide intermediate. 10-Undecenylamine spacer and its 10-undecenamide intermediate were synthesised using the procedure described elsewhere.[27] The full characterization of these compounds was not reported previously, being therefore presented here.

10-Undecenamide, white crystals (81% yield); mp 85–87 °C ($CHCl_3$/*n*-hexane) (mp lit.[27] 88.5–89 °C); IR (KBr, cm^{-1}): 3359 (NH), 3192 (NH), 3083, 2922, 2851, 1662 (CONH), 1632 (C=C), 1469, 1426, 1420, 912, 702, 637; ^{1}H NMR ($CDCl_3$): δ 1.30 (10 H, s, CH_2), 1.63 (2H, m, CH_2CH_2C=O), 2.04 (2H, m, CH_2CH=CH_2), 2.22 (2H, t, $J = 7.5$ Hz, CH_2C=O), 4.93 (1H, br d, $J_{11,10(cis)} = 10.2$ Hz, *H*CH=CH), 4.99 (1H, dd, $J_{11,10(trans)} = 17.1$ and $J_{gem} = 1.5$ Hz, HC*H*=CH), 5.44 (1H, br s, N–H, D_2O exchange), 5.61 (1H, br s, N–H, D_2O exchange), 5.82 (1H, dddd, $J_{10,11(trans)} = 17.1$, $J_{10,11(cis)} = 10.2$ Hz, $J_{10,9} = 6.9$ and 6.9 Hz, C*H*=CH_2); EIMS *m*/*z* (relative intensity) 183 $[M]^+$ (24.3), 141 (18.2), 123 (12.2), 111 (15.3), 97 (14.2), 83 (5.7), 59 $[H_2NC(OH)CH_2]^+$ (84.3), 44 $[H_2NCO]^+$ (28.5), 43 (100).

10-Undecenylamine, colourless oil (76.3% yield), bp 106 °C, 10 mmHg (bp lit.[27] 123–124 °C, 21 mmHg); IR (NaCl cell, cm^{-1}): 3330 (NH), 3080, 2920, 2850, 1640 (C=C), 1570, 1480, 1470, 1150, 990, 910; ^{1}H NMR ($CDCl_3$): δ 1.28 (12H, s, CH_2), 1.44 (2H, t, $J = 6.9$ Hz, $CH_2CH_2NH_2$), 2.04 (2H, m, CH_2CH_2=CH_2), 2.68 (2H, t, $J = 6.9$ Hz, CH_2NH_2), 4.93 (1H, br d, $J_{11,10(cis)} = 10.2$ Hz, *H*CH=CH), 4.99 (1H, dd, $J_{11,10(trans)} = 17.1$ and $J_{gem} = 1.5$ Hz, HC*H*=CH), 5.82 (1H, dddd, $J_{10,11(trans)} = 17.1$, $J_{10,11(cis)} = 10.2$ Hz, $J_{10,9} = 6.9$ and 6.9 Hz, C*H*=CH_2); EIMS *m*/*z* (relative intensity): 169 $[M]^+$ (30.0), 88 (10.3), 70 (20.4), 61 (40.2), 43 $[CH_2CHNH_2]^+$ (100).

4.3.2. Dehydroabietoyl chloride, 4. Dehydroabietic acid (0.99 g, 3.29 mmol) dissolved in $SOCl_2$ was heated under reflux (6 h). The excess of $SOCl_2$ was evaporated under reduced pressure and the crude product was washed successively with toluene (40 mL). A yellow crystalline product **4** was obtained, mp 150–152 °C (toluene); $[\alpha]_D^{23} = +59.0$ (*c* 1, ethanol); IR (KBr, cm^{-1}): 3060, 2900, 2850, 1780 (C=OCl), 1530, 1460, 1420, 990, 914; ^{1}H NMR ($CDCl_3$): δ 1.14 (3H, s, CH_3-20), 1.15 (6H, d, $J = 6.9$ Hz, CH_3-16

and 17), 1.30 (3H, s, CH_3-19), 1.51 (2H, m, H-1_{ax} and H-6_{ax}), 1.72 (5H, m, 2H-2, 2H-3 and H-6_{eq}), 2.13 (1H, br d, $J = 12.6$ Hz, H-5), 2.27 (1H, m, H-1_{eq}), 2.86 (3H, m, 2H-7 and H-15), 6.83 (1H, s, H-14), 7.01 (1H, dd, $J_{12,14} = 1.2$ and $J_{12,11} = 8.1$ Hz, H-12), 7.10 (1H, d, $J_{11,12} = 8.1$ Hz, H-11); EIMS *m/z* (relative intensity, %): 320 $[M+2]^+$ (2.0), 318 $[M]^+$ (6.6), 303 $[M-CH_3]^+$, (12.0), 255 $[M-COCl]^+$ (35.0), 43 $[CH(CH_3)_2)]^+$ (100).

4.3.3. *N*-(10′-Undecenyl)dehydroabietamide, 5. Dehydroabietoyl chloride (0.04 g, 0.13 mmol) dissolved in dry toluene (3 mL) was added to a vigorously stirred solution of 10-undecenylamine (0.45 g, 0.66 mmol) in toluene (3 mL). Subsequently, the mixture was stirred for 48 h at room temperature. The solvent was evaporated under reduce pressure and the crude product (1.9 g) was purified by column chromatography on silica gel using petroleum ether/dichloromethane (2:1) as an eluent, affording a colourless oil of *N*-(10′-undecenyl)dehydroabietamide **5** (0.05 g, 93% yield); $[\alpha]_D^{23} = +57.7$ (*c* 1, ethanol); IR (NaCl cell, cm^{-1}): 3350 (NH), 3060, 2900–2840, 1640 (C=O, amide), 1530, 1460, 1380, 1360, 1270, 900, 810; ^1H NMR ($CDCl_3$): δ 1.21 (6H, d, $J = 6.9$ Hz, CH_3-16 and 17), 1.22 (3H, s, CH_3-20), 1.26 (3H, s, CH_3-19), 1.28 (12H, s, H-3′ to H-8′), 1.51 (4H, m, H-2′, H-1_{ax} and H-6_{ax}), 1.73 (5H, m, 2H-2, 2H-3 and H-6_{eq}), 2.05 (2H, q, $J = 6.9$ Hz, H-9′), 2.12 (1H, dd, $J_{5ax6eq} = 1.8$ and $J_{5ax6ax} = 12.3$ Hz, H-5), 2.30 (1H, br d, $J = 12.9$ Hz, H-1_{eq}), 2.87 (3H, m, 2H-7 and H-15), 3.24 (2H, m, H-1′), 4.88 (1H, br d, $J_{11',10'(cis)} = 10.2$ Hz, CH_2=CH), 4.90 (1H, dd, $J_{11',10'(trans)} = 17.1$ and $J_{gem} = 1.5$ Hz, CH_2=CH), 5.82 (2H, m, H-10′ and N–H, D_2O exchange), 6.86 (1H, d, $J_{14,12} = 1.2$ Hz, H-14), 7.00 (1H, dd, $J_{12,14} = 1.2$ and $J_{12,11} = 8.1$ Hz, H-12), 7.16 (1H, d, $J_{11,12} = 8.1$ Hz, H-11); ^{13}C NMR ($CDCl_3$): δ 39.76 (C-1), 18.73 (C-2), 37.26 (C-3), 47.14 (C-4), 45.54 (C-5), 21.04 (C-6), 26.91 (C-7), 134.58 (C-8), 146.97 (C-9), 37.96 (C-10), 123.98 (C-11), 123.81 (C-12), 145.61 (C-13), 126.81 (C-14), 33.40 (C-15), 23.92 (C-16 and C-17), 178.12 (C-18), 16.48 (C-19), 25.17 (C-20), 37.03 (C-1′), 29.96 (C-2′), 29.60 (C-3′), 29.43 (C-4′), 29.35 (C-5′), 29.22 (C-6′), 29.05 (C-7′), 28.87 (C-8′), 33.74 (C-9′), 139.10 (C-10′), 114.09 (C-11′); EIMS *m/z* (relative intensity, %): 451 $[M]^+$ (88.1), 437 $[M-14]^+$ (87.0), 436 $[M-15]^+$ (6.2%), 282 (8.3), 255 (23.8), 267 $[M-NH_2(CH_2)_9CHCH_2-CH_3]^+$ (5.0), 239 $[M-CONH_2(CH_2)_9-CHCH_2-CH_3]^+$ (82.3), 225 $[M-CONH(CH_2)_9CHCH_2]^+$ (23.8), 199 (15.6), 185 (36.4), 173 (100), 159 (27.5), 131 (25.1), 109 (23.4), 81 (18.4), 69 (33.3), 55 (39.4), 43 (30.0), 41 (20.3); HRMS (ESI) *m/z*: 452.388 $[M+H]^+$ (calculated for $C_{31}H_{49}NO$, 452.389).

4.3.4. *N*-[11′-(Chlorodimethylsilyl)undecyl]dehydroabietamide, 6. A solution of **5** (0.12 g, 0.27 mmol) in 5 mL dry dichloromethane was added to a stirred solution of chloroplatinic acid in propan-2-ol (0.1 mL, 0.13 mmol/mL) and the mixture was stirred at room temperature. Then, dimethylchlorosilane (0.3 mL) was added and the mixture was heated under reflux for 4 h and 30 min. The solvent and excess silane were eliminated under reduced pressure leading to the *N*-[11′-(chlorodimethylsilyl)undecyl]dehydroabietamide **6** (0.14 g, 99% yield) as a brownish gum, used without further purification. IR (NaCl cell, cm^{-1}): 3300 (NH), 3080, 2930, 1630 (C=O), 1467, 1380, 1254 (Si–C), 1058 (Si–O–C), 830 (Si–O), 800 (Si–C); ^1H NMR ($CDCl_3$): δ 0.54 (6H, sl, $(CH_3)_2Si$), 0.81 (2H, m, H-11′-Si), 1.21 (6H, d, $J = 6.9$ Hz, CH_3-16 and 17), 1.22 (3H, s, CH_3-20), 1.26 (3H, s, CH_3-19), 1.27 (12H, s, H-3′–8′), 1.54 (4H, m, H-2′, H-1_{ax} and H-6_{ax}), 1.75 (4H, m, 2H-2 and 2H-3), 2.13 (1H, br d, $J = 12.6$ Hz, H-5), 2.32 (1H, br d, $J = 12.6$ Hz, H-1_{eq}), 2.84 (3H, m, H-15 and H-7), 3.22 (2H, m, H-1′), 5.72 (1H, br s, NH, D_2O exchange), 6.86 (1H, d, $J_{14,12} = 1.2$ Hz, H-14), 7.00 (1H, dd, $J_{12,14} = 1.2$ and $J_{12,11} = 8.1$ Hz, H-12), 7.16 (1H, d, $J_{11,12} = 8.1$ Hz, H-11); ^{13}C NMR ($CDCl_3$): δ 39.45 (C-1), 18.36 (C-2), 36.87 (C-3), 46.79 (C-4), 45.14 (C-5), 20.68 (C-6), 26.59 (C-7), 134.30 (C-8), 146.60 (C-9), 37.58 (C-10), 123.65 (C-11), 123.45 (C-12), 145.27 (C-13), 126.46 (C-14), 33.04 (C-15), 23.58 (C-16 and C-17), 177.84 (C-18), 16.13 (C-19), 24.84 (C-20), 36.66 (C-1′), 29.61 (C-2′), 29.24 (C-3′ and C-4′), 29.03 (C-5′), 28.93 (C-6′), 33.09 (C-8′), 22.89 (C-10′), 18.02 (C-11′), 1.60 (CH_3–Si); EIMS *m/z* (relative intensity, %): 460 $[M-85]^+$ (9.0), 454 (61.7), 451 $[M-HSi(CH_3)_2Cl]^+$ (7.8), 452 $[M-Si(CH_3)_2Cl]^+$ (17.4), 438 $[M-CH_2Si(CH_3)_2Cl]^+$ (45.5), 282 $[M-NH_2-(CH_2)_{11}Si(CH_3)_2Cl]^+$ (8.1), 267 $[M-NH_2(CH_2)_{11}Si(CH_3)_2-Cl-CH_3]^+$ (3.3), 255 (28.2), 239 $[M-CONH_2(CH_2)_{11}-Si(CH_3)_2Cl-CH_3]^+$ (72.4), 199 (15.9), 185 (40.0), 173 (100), 159 (27.9), 131 (24.0), 117 (15.9), 109 (19.9), 97 (17.3), 95 (18.8), 93 $[Si(CH_3)_2Cl]^+$ (5.8), 83 (15.2), 81 (18.9), 69 (2.5), 55 (43.8), 43 $[CH(CH_3)_2]^+$ (53.8), 41 (28.2).

4.3.5. Chemically bonded CSP 1 and HPLC column packing. A solution of **6** (1 g, 1.84 mmol) in dry toluene (8 mL) was added dropwise to silica gel (2.063 g, Nucleosil 100-5) previously dried at 120 °C under high vacuum for 30 h. The mixture was gently stirred at reflux. The solvent was removed by evaporation under reduce pressure and the modified silica was kept in a high vacuum oven at 100 °C for 24 h. The bonded phase was then washed and filtered successively with toluene, methanol, acetone and *n*-hexane. Elemental analysis of modified silica gel **CSP 1** (C, 16.33; H, 2.60; N, 0.30) showed a loading of 0.22 mmol of the chiral selector (based on C) or 0.24 mmol (based on N) per gram of stationary phase. The bonded phase was slurried in methanol and packed in a 100×4.6 mm ID stainless-steel HPLC column using a conventional slurry packing method. A solution of 2 mL of hexamethyldisilazane in 50 mL of dichloromethane was eluted through the column to endcapping the remaining free silanol groups of the bonded phase. Then the unreacted hexamethyldisilazane was removed out washing the column with 100 mL of dichloromethane.[33]

4.4. Synthesis of CSP 2

12,14-Dinitrodehydroabietic acid **2** was obtained by nitration of dehydroabietic acid **1**[31] and **CSP 2** was prepared similarly to the procedure described above for **CSP 1**.

4.4.1. 12,14-Dinitrodehydroabietoyl chloride, 7. Compound **7**, prepared following the procedure described in Section 4.3.2, was obtained as yellow crystals in an 85% yield; mp 157–160 °C (Et_2O); $[\alpha]_D^{23} = +47.5$ (*c* 1, acetone); IR (KBr, cm^{-1}): 2955, 2870, 1789 (C=O), 1498, 1460,

1419, 994, 914; ^{1}H NMR ($CDCl_3$): δ 1.26 (3H, s, CH_3-20), 1.32 (6H, d, $J = 6.9$ Hz, CH_3-16 and 17), 1.39 (3H, s, CH_3-19), 1.54 (2H, m, H-1_{ax} and H-6_{ax}), 1.88 (5H, m, 2H-2, 2H-3, H-6_{eq}), 2.26 (1H, br d, $J = 13.6$ Hz, H-1_{eq}), 2.30 (1H, dl, $J = 12.1$ Hz, H-5), 2.82 (2H, m, 2H-7), 3.03 (1H, hept, $J = 6.9$ Hz, H-15), 7.54 (1H, s, H-11); EIMS *m/z* (relative intensity, %): 410 $[M+2]^+$ (1.8), 408 $[M]^+$ (4.9), 393 $[M-CH_3]^+$ (14.7), 391 $[M-OH]^+$ (36.5), 329 $[M-(CO+HCl)]^+$ (55.7), 263 (45.4), 43 $[CH(CH_3)_2]^+$ (100).

4.4.2. *N*-(10′-Undecenyl)-12,14-dinitrodehydroabietamide, 8. Compound **8**, prepared following the procedure described in Section 4.3.3 was obtained as a yellow oil in an 86% yield; $[\alpha]_D^{23} = +36.9$ (*c* 1, acetone); IR (NaCl cell, cm^{-1}): 3367 (NH), 3075, 2927, 2855, 1631 (C=O), 1536 (NO), 1466, 1365 (NO), 961, 750, 735; ^{1}H NMR ($CDCl_3$): δ 1.24 (3H, s, CH_3-20), 1.26 (3H, s, CH_3-19), 1.28 (12H, s, H-3′–8′), 1.31 (6H, d, $J = 6.9$ Hz, CH_3-16 and 17), 1.53 (5H, m, H-1_{ax}, 2H-6 and 2H-2′), 1.76 (4H, *m*, 2H-2 and 2H-3), 2.03 (2H, *q*, $J = 6.9$ Hz, H-9′), 2.23 (2 H, m, H-1_{eq} and H-5), 2.85 (2H, m, 2H-7), 3.02 (1H, hept, $J = 6.9$ Hz, H-15), 3.26 (2H, q, $J = 7.2$ Hz, H-1′), 4.88 (1H, br d, $J_{11',10'(cis)} = 10.2$ Hz, *H*CH=CH), 4.90 (1H, dd, $J_{11',10'(trans)} = 17.1$ and $J_{gem} = 1.5$ Hz, HC*H*=CH), 5.82 (2H, m, H-10′ and NH, D_2O exchange), 7.54 (1H, s, H-11); ^{13}C NMR ($CDCl_3$): δ 37.64 (C-1), 18.32 (C-2), 36.74 (C-3), 46.73 (C-4), 43.54 (C-5), 20.54 (C-6), 24.50 (C-7), 130.62 (C-8), 151.03 (C-9), 37.52 (C-10), 121.21 (C-11), 149.24 (C-12), 139.02 (C-13), 151.87 (C-14), 33.77 (C-15), 20.61 (C-16), 20.64 (C-17), 177.20 (C-18, C=O amide), 16.56 (C-19), 24.90 (C-20), 39.92 (C-1′), 29.57, 29.46, 29.37, 29.23, 29.06, 28.95, (7C, C-2′ to C-8′ of aliphatic chain), 26.94 (C-9′), 139.02 (C-10′), 113.99 (C-11′); EIMS *m/z* (relative intensity, %): 541 $[M]^+$ (19.0), 526 $[M-CH_3]^+$ (54.3), 524 $[M-OH]^+$ (37.8), 329 $[M-(CONH_2(CH_2)_9-CHCH_2+CH_3)]^+$ (19.4), 313 (7.6), 289 (1.7), 275 (13.0), 263 (49.1), 249 (4.8), 238 (24.5), 224 (9.6), 55 (100), 43 $[CH(CH_3)_2]^+$ (72.4), 41 (75.7); HRMS(EI) *m/z*: 540.343898 $[M-H]^-$ (calculated for $C_{31}H_{46}N_3O_5$ 540.344296).

4.4.3. *N*-[11′-(Chlorodimethylsilyl)undecyl]-12,14-dinitrodehydroabietamide, 9. Compound **9**, prepared using the procedure described in Section 4.3.4 was isolated as a yellow oil in a quantitative yield; IR (NaCl cell, cm^{-1}): 3300 (NH), 3075, 2926, 2855, 1631 (CO), 1536 (NO), 1467, 1368 (NO), 1255 (Si–C), 1059 (Si–O–C), 909, 840 (Si–O), 799 (Si–C), 735; ^{1}H NMR ($CDCl_3$): δ 0.40 (6H, br s, Si–$(CH_3)_2$), 0.83 (2H, m, H-11′), 1.29 (3H, s, CH_3-19), 1.27 (12H, s, H-3′–8′), 1.24 (3H, s, CH_3-20), 1.30 (6H, d, $J = 7.2$ Hz, CH_3-16 and 17), 1.56 (5H, m, H-1_{ax}, 2H-6 and H-2′), 1.78 (4H, m, 2H-2 and 2H-3), 2.24 (2 H, m, H-1_{eq} and H-5), 2.75 (2H, m, 2H-7), 3.01 (1H, hept, $J = 6.9$ Hz, H-15), 3.22 (2H, q, $J = 7.2$ Hz, H-1′), 6.04 (1H, br s, NH, D_2O exchange), 7.55 (1H, s, H-11); ^{13}C NMR ($CDCl_3$): δ 37.63 (C-1), 18.28 (C-2), 36.59 (C-3), 46.76 (C-4), 43.47 (C-5), 19.53 (C-6), 24.47 (C-7), 130.63 (C-8), 151.04 (C-9), 37.42 (C-10), 121.30 (C-11), 149.35 (C-12), 128.33 (C-13), 151.96 (C-14), 32.91 (C-15), 20.62 (C-16), 20.53 (C-17), 177.60 (C-18, C=O amide), 16.58 (C-19), 24.88 (C-20), 40.14 (C-1′), 29.50, 29.43, 29.22, 28.94, 26.91 (7C of aliphatic chain, C-2′ to C-8′), 22.93, (C-10′), 18.94 (C-11′), 1.65 (CH_3–Si); EIMS *m/z* (relative intensity, %): 637 $[M+2]^+$ (1.2), 635 $[M]^+$ (28.1), 619 (25.9), 617 $[M-H_2O]^+$ (33.6), 601 (30.0), 541 $[M-HSi(CH_3)_2Cl]^+$ (22.2), 525 $[M-(OH+Si(CH_3)_2Cl)]^+$ (89.3), 508 (14.6), 329 (6.6), 328 (13.1), 312 (9.4), 289 (1.5), 263 (19.6), 262 (40.4), 247 (26.0), 93 (100), 83 (23.6), 69 (46.8), 55 (60.9), 43 $[CH(CH_3)_2]^+$ (40.5), 41 (32.8).

4.4.4. Chemically bonded CSP 2. The covalent linkage of chiral selector **9** to silica gel was carried out following a similar procedure described above for **CSP 1**. Elemental analysis of **CSP 2** (found: C, 14.26; H, 2.30; N, 1.29) gave a loading of 0.36 mmol of selector (based on C) or 0.31 mmol (based on N) per gram of stationary phase. The bonded phase was slurried in methanol and packed in a 150×4.6 mm ID stainless steel HPLC column using a conventional slurry packing method. Endcapping of modified silica was carried out using the procedure detailed in Section 4.3.5.

4.5. Synthesis of CSP 3

4.5.1. 4′-(Chlorocarbonyl)-1′-friedelan-3α-yl-benzoate, 10. Friedelan-3α-ol **3a** (0.28 g, 0.65 mmol) dissolved in dry toluene (25 mL) was added to tereftaloyl chloride (0.599 g, 2.97 mmol) and 4-dimethylaminepyridine (4-DMAP) (0.125 g, 1.03 mmol) and then the mixture was heated under reflux for 8 h. The toluene was removed under reduced pressure and the residue was used in the next reaction without purification.

4.5.2. 4′-(*N*-10″-Undecenylamide)-1′-friedelan-3α-yl-benzoate, 11. 10-Undecenylamine (0.133 g, 0.79 mmol) in 5 mL ether was added to a solution of **10** in dry pyridine (0.5 mL) at 0 °C and the mixture was stirred at room temperature for 2 h. The solvent was evaporated under reduced pressure and the white crude product obtained was purified by column chromatography on silica gel using dichloromethane/methanol (1%) as the eluent affording 0.211 g of **11** in a 45% yield. Mp 218–220 °C; $[\alpha]_D^{23} = -6.4$ (*c* 0.94, CH_2Cl_2); IR (KBr, cm^{-1}): 3402 (NH), 2926, 2855, 2870, 1715 (C=O ester), 1642 (C=C and C=O amide), 1545, 1437, 1278; ^{1}H NMR ($CDCl_3$): δ 0.83 (3H, d, $J = 6.3$ Hz, CH_3-23), 0.85 (3H, s, CH_3-24), 0.89 (3H, s, CH_3-25), 0.96 (3H, s, CH_3-30), 1.01 (6H, s, CH_3-27 and CH_3-29), 1.03 (3H, s, CH_3-26), 1.17 (3H, s, CH_3-28), 1.28 (14H, s, H-2″ to H-8″), 2.04 (2H, dt, $J = 6.5$ and 7.3 Hz, H-9″), 2.23 (1H, m, H-4), 3.47 (2H, q, $J = 6.7$ Hz, H-1″), 4.96 (3H, m, H-3 and 2H-11″), 5.84 (1H, m, H-10″), 6.29 (1H, t, $J = 5.1$ Hz, NH, D_2O exchange), 7.82 (2H, d, J=8.1 Hz, Ar–H-3′ and Ar–H-5′), 8.07 (2H, d, $J = 8.1$ Hz, Ar–H-2′ and Ar–H-6′); ^{13}C NMR ($CDCl_3$): δ 19.31 (C-1), 32.62 (C-2), 76.40 (C-3), 50.10 (C-4), 38.25 (C-5), 41.28 (C-6), 17.8 (C-7), 52.96 (C-8), 36.97 (C-9), 59.85 (C-10), 35.51 (C-11), 30.51 (C-12), 39.62 (C-13), 38.45 (C-14), 32.75 (C-15), 35.98 (C-16), 29.95, (C-17), 42.75 (C-18), 35.27 (C-19), 28.12 (C-20), 32.29 (C-21), 39.19 (C-22), 10.10 (C-23), 14.50 (C-24), 18.1 (C-25), 18.60 (C-26), 20.10 (C-27), 32.05 (C-28), 31.74 (C-29), 34.96 (C-30), 133.32 (C-1′), 126.77 (C-2′), 129.65 (C-3′), 138.47 (C-4′), 129.65 (C-5′), 126.77 (C-6′), 40.20 (C-1″), 29.56, 29.42, 29.33, 29.23, 29.03, 28.84 (C-

2″–C-7″), 26.94 (C-8″), 33.74 (C-9″), 139.12 (C-10″), 114.09 (C-11″), 166.59 (C=O amide), 165.50 (C=O ester); FAB-MS (NBA) *m/z* (relative, intensity %): 729 $[M+1]^+$ (30.9), 559 $[M-NH(CH_2)_9CHCH_2]^+$ (9.2), 485 (5.8), 411 (11.0), 374 (6.4), 318 (100), 300 (38.9), 297 (8.9). Elemental analysis calculated for $C_{49}H_{77}NO_3$: C, 80.89; H, 10.69; N, 2.01. Found: C, 80.83; H, 10.66; N, 1.93.

4.5.3. *N*-[11′-(Chlorodimethylsilyl)undecyl]-1′-friedelan-3α-yl-benzoate, 12. Compound **12** was prepared using the procedure reported in Section 4.3.4 and isolated as a yellow oil in a quantitative yield. ^{1}H NMR ($CDCl_3$): δ 0.39 (6H, br s, Si–(CH_3)$_2$), 0.82 (3H, d, $J = 6.6$ Hz, Me-23), 0.84 (3H, s, Me-24), 0.88 (3H, s, Me-25), 0.94 (3H, s, Me-29), 0.99 (6H, s, Me-27 and Me-30), 1.02 (3H, s, Me-26), 1.17 (3H, s, Me-28), 1.27 (12H, s, $(CH_2)_6''$), 3.46 (2H, m, H-1″), 4.89 (1H, m, H-3), 6.13 (1H, br s, NH, D_2O exchange), 7.82 (2H, d, $J = 8.4$ Hz, H-2′ and H-6′), 8.07 (2H, d, $J = 8.4$ Hz, H-3′ and H-5′).

4.5.4. Chemically bonded CSP 3. Covalent linkage of chiral selector **12** to silica gel was undertaken using the procedure described in Section 4.3.5. Elemental analysis of CSP 3 (Found: C, 14.71; H, 2.67; N, 0.32) showed a loading of 0.24 mmol of selector (based on C) or 0.23 mmol (based on N) per gram of stationary phase. The modified silica was packed into a 100×4.6 mm ID stainless-steel HPLC column and the endcapping of modified silica was carried out following the procedure described in Section 4.3.5.

4.6. Molecular modelling

The molecular modelling studies were performed through molecular mechanics (MM) and MD simulations using the AMBER 8 software suite[41] with parameters taken from the GAFF force field, of general use for organic molecules.[42] Partial atomic charges were calculated using the AM1-BCC bond charge correction model[43] as implemented in AMBER 8.

The structures of the two binaphthol atropisomers **14** were retrieved from their crystal structures available from Cambridge Structural Data Base[44] while the structures of the amino acids as well as the structures of the chiral selectors of **CSP 1** and **CSP 2** were built by manipulation of the atomic coordinates of the structures of related compounds deposited on this data base. For example, the selectors of both chiral stationary phases were generated from dehydroabietic acid **1** structure with the silica gel support omitted and the $-(CH_2)_{11}SiMe_2$ spacer replaced by a terminal *n*-propyl group. The starting geometries of all binary selector–analyte binding associations (diastereomeric complexes) were obtained by quenched molecular dynamics using the following methodology. The (*R*) and (*S*) enantiomers of two racemic amino acids, **17a** and **17d**, were docked separately to the selectors of **CSP 1** and **CSP 2** leading to eight independent diastereomeric structures. Subsequently, all (*R*) and (*S*) complexes were minimised by MM and subject to MD runs of 2 ns at 2000 K using a relaxation time step of 1 fs. Frames were collected at 0.2 ps intervals of simulation leading to a trajectory file containing 20,000 structures, which were then fully minimised by MM using an appropriated Python in-house script. The lowest energy structures found for each complex were used as starting geometries in further MD runs carried out for 40 ns in the gas phase. Frames were saved every 0.1 ps of simulation giving arise to a trajectory files containing 400,000 structures. The kinetic energy of the systems was kept constant coupling the system to a Langevin thermostat with a collision frequency of 1.0 ps^{-1}. All nonbonded interactions were evaluated applying a virtually infinite cut-off of 99 Å. In order to keep the analyte and the selector together a weak restraint distance using a force constant of 5.0 kcal mol^{-1} was applied when the distance between the chiral centre of the analytes and C-4 chiral carbon from stationary phases was higher than 10.0 Å using a parabolic function as defined in AMBER 8. Otherwise the selector and the analyte showed a tendency to separate.

The MD simulations in explicit solvent were carried in equilibrated cubic boxes composed of *n*-hexane and propan-2-ol molecules in a ratio consistent with the *n*-hexane/propan-2-ol solvent mixture (80:20 v/v) used in HPLC separations. The solvent molecules were simulated using all atom models with parameters taken from the GAFF force field and ESP atomic charges calculated at the RHF/6-31G* level.[45] An individual cubic box composed of 64 propan-2-ol molecules was built replicating a single molecular mechanics minimized propan-2-ol molecule with the Vega software.[46] The same procedure was adopted to generate a cubic box having 155 *n*-hexane solvent molecules. Subsequently, the two boxes were merged yielding the *n*-hexane/propan-2-ol mobile phase. This new cubic box was input into AMBER 8 and minimised by MM in order to remove bad intermolecular contacts. Then, the system was heated at 300 K with a NVT ensemble for 200 ps, followed of a NPT molecular dynamics run of 400 ps at an average pressure of 1 atm. At the end of this simulation, the cubic box displayed a density of 0.607 g cm^{-3}, which is within the range of expected values for the experimental density of *n*-hexane/propan-2-ol solvent mixture (80:20 v/v). Furthermore, the majority of propan-2-ol solvent molecules are self-assembled in supramolecular aggregates stabilized by O–H···O hydrogen bonds interactions. Indeed, the equilibrated box exhibited four propan-2-ol molecules separated from others as well as small isolated solvent clusters composed of three tetramers and five dimers. The remaining propan-2-ol molecules were involved in the formation of a large solvent network. Therefore, in order to obtain a more regular distribution of the alcohol molecules into the solvent box, the system was subsequently heated at 500 K for 200 ps using a NVT ensemble. The last frame saved for this simulation displayed an effective dispersion of solvent molecules containing only nine dimers and one trimer of propan-2-ol molecules. This frame was then minimized by molecular mechanics and subsequently used to solvate separately the two **CSP 1**. Compound **17a** diastereomeric complexes. The final cubic boxes composed of one complex surrounded by 62 propan-2-ol and 142 *n*-hexane molecules were obtained. Each system was then equilibrated using a multistage protocol. The equilibration process started with minimisation of the solvent molecules by MM with 500 steps by the steepest descent method followed by 2000 steps

of conjugate gradients keeping the structure of the solute diastereomeric complex with positional restraints of 500 kcal mol^{-1} $Å^{-2}$. Then, the restraint was removed and the system was allowed to relax using an identical molecular mechanics protocol. The equilibration then continued with the heating of the system at 300 K for 400 ps using a NPT ensemble and a weak positional restraint of 5 kcal mol^{-1} $Å^{-2}$ on the solute. Finally, the restraint was removed and a NPT molecular dynamics run of 50 ps at average pressure of 1 atm was carried out. At the end of this simulation the density was within the expected value for *n*-hexane/propan-2-ol solvent liquid mixture (80:20 v/v) reported above. Data collection runs in a NPT ensemble at 300 K and 1 atm were performed over 4 ns from the equilibrated structures of the solvated diastereomeric complexes.

All simulations in explicit solvent were carried out under periodic boundary conditions using a time step of 2 fs. Bond lengths involving hydrogen bonded atoms were constrained with SHAKE algorithm.[47] The particle Mesh Ewald method was used to treat the long-range electrostatic interactions and non-bonded van der Waals interactions were truncated with a 12 Å cut-off. The temperature of the bath was controlled with a Langevin thermostat using a collision frequency of 1.0 ps^{-1}.

The binding interaction energy terms, given in Table 2, were calculated by post-processing the trajectory files of simulations obtained for each diastereomeric complex with the MM-PBSA method.[37] Snapshots of the isolated diastereomeric complexes were taken from the MD trajectory file at intervals at 0.2 ps. A total of 200,000 frames were produced and subsequently used on the calculation of the average energies.

Molecular graphics were drawn with Pymol[48] or Chimera[49] visualization systems.

Acknowledgements

The authors thank Professor Q. Cass from Departamento de Química da Universidade Federal de São Paulo, Brazil for the packing of the HPLC columns. N.F. also acknowledges FCT a Grant (SFRH/BD/25117/2005).

References

1. Caldwell, J. *J. Chromatogr. A* **1996**, *719*, 3–13.
2. Maier, N. M.; Franco, P.; Lindner, W. *J. Chromatogr. A* **2001**, *906*, 3–33.
3. Lai, X.; Ng, S.-C. *Tetrahedron Lett.* **2003**, *44*, 2657–2660.
4. Stalcup, A. M. In *A Practical Approach to Chiral Separations by Liquid Chromatography*; 1st ed.; Subramanian, G., Ed., Wiley-VCH: Weinheim, 1994, Chapter 5.
5. Yashima, E. *J. Chromatogr. A* **2001**, *906*, 105–125.
6. Haginaka, J. *J. Chromatogr. A* **2001**, *906*, 253–273.
7. Ward, T. J.; Farris, A. B., III. *J. Chromatogr. A* **2001**, *906*, 73–89.
8. Hui, F.; Ekborg-Ott, K. H.; Armstrong, D. W. *J. Chromatogr. A* **2001**, *906*, 91–103.
9. Beesley, T. E.; Lee, J. T.; Wang, A. X. In *Chiral Separation Techniques. A Practical Approach*; 2nd ed.; Subramanian, G., Ed., Wiley-VCH: Weinheim, 2001, Chapter 2.
10. Nakano, T. *J. Chromatogr. A* **2001**, *906*, 205–225.
11. Sellergren, B. *J. Chromatogr. A* **2001**, *906*, 227–252.
12. Hirose, K.; Yongzhu, J.; Nakamura, T.; Nishioka, R.; Ueshige, T.; Tobe, Y. *J. Chromatogr. A* **2005**, *1078*, 35–41.
13. Pirkle, W. H.; Pochapsky, T. C. *Chem. Rev.* **1989**, *89*, 347–362.
14. (a) Gasparrini, F.; Misiti, D.; Villani, C. *J. Chromatogr. A* **2001**, *906*, 35–50; (b) Francotte, E. R. *J. Chromatogr. A* **2001**, *906*, 379–397.
15. Welch, C. J. *J. Chromatogr. A* **1994**, *666*, 3–26.
16. Welch, C. J. In *Crawling out of the Chiral Pool The Evolution of Pirkle-Type Chiral Stationary Phases*; Brown, Phyllis R., Grushka, Eli, Eds.; Advances in Chromatography; Marcel Dekker: New York, 1995; Vol. 35, Chapter 4, pp 171–197.
17. Rosini, C.; Altemura, P.; Pini, D.; Bertucci, C.; Salvadori, P.; Zullino, G. *J. Chromatogr. A* **1985**, *348*, 79–87.
18. Sinibaldi, M.; Flieger, M.; Cvak, L.; Messina, A.; Pichini, A. *J. Chromatogr. A* **1994**, *666*, 471–478.
19. Dondi, M.; Olsovska, J.; Flieger, M.; Sinibaldi, M.; Polcaro, C. M. *J. Chromatogr. A* **1999**, *859*, 133–142.
20. Mandl, A.; Nicoletti, L.; Lämmerhofer, M.; Lindner, W. *J. Chromatogr. A* **1999**, *858*, 1–11.
21. Krawinkler, K. H.; Maier, N. M.; Sajovic, E.; Lämmerhofer, M.; Lindner, W. *J. Chromatogr. A* **2004**, *1053*, 119–131.
22. Franco, P.; Lämmerhofer, M. M.; Klaus, P.; Lindner, W. *J. Chromatogr. A* **2000**, *869*, 111–127.
23. Iuliano, A.; Salvadori, P.; Félix, G. *Tetrahedron: Asymmetry* **1999**, *10*, 3353–3364.
24. Iuliano, A.; Félix, G. *J. Chromatogr. A* **2004**, *1031*, 187–195.
25. Iuliano, A.; Ruffini, A. *Tetrahedron: Asymmetry* **2005**, *16*, 3820–3828.
26. Machida, Y.; Nishi, H.; Nakamura, K.; Nakai, H.; Sato, T. *J. Chromatogr. A* **1997**, *757*, 73–79.
27. Dobashi, Y.; Hara, S. *J. Org. Chem.* **1987**, *52*, 2490–2496.
28. Halbrook, J.; Lawrence, R. *J. Org. Chem.* **1966**, *31*, 4246–4247.
29. Moiteiro, C.; Justino, F.; Tavares, M. R.; Curto, M. J. M.; Florêncio, M. H.; Pinto, M. M.; Pedro, M.; Nascimento, M. S. J.; Cerqueira, F. *J. Nat. Prod.* **2001**, *64*, 1273–1277.
30. Moiteiro, C.; Curto, M. J. M.; Mohamed, N.; Martínez-Díaz, M. B. R.; Coloma, A. G. *J. Agric. Food Chem.* **2006**, *54*, 3566–3571.
31. Fieser, R. F.; Campbell, W. P. *J. Am. Chem. Soc.* **1938**, *60*, 159–170.
32. Moiteiro, C.M.; Tavares, M.R.; Lobo, A.M.; Curto, M.J.M. Instituto Nacional de Engenharia e Tecnologia Industrial, Application Patent PT102878, 2004.
33. Pirkle, W. H.; Readnour, R. S. *Chromatographia* **1991**, *31*, 129–132.
34. Pirkle, W. H.; Liu, Y. *J. Chromatogr. A* **1996**, *736*, 31–38.
35. Merck Chrombook, 2nd ed.; Merck: Darmstadt, Germany, 1998; p 117.
36. Lin, C. E.; Lin, C. H.; Li, F. K. *J. Chromatogr. A* **1996**, *722*, 189–198.
37. Kollman, P. A.; Massova, I.; Kuhn, B.; Huo, S.; Chong, L.; Lee, M.; Lee, T.; Duan, Y.; Wang, W.; Cieplak, P.; Donni, O.; Srinivasan, J.; Case, D. A.; Cheatham, T. E., Jr. *Acc. Chem. Res.* **2000**, *33*, 889–897.
38. Lipkowitz, K. *Acc. Chem. Res.* **2000**, *33*, 555–562.
39. Zhang, Y.; Wu, D.; Wang-Iverson, D. B.; Tymiak, A. A. *Drug Discovery Today* **2005**, *10*, 571–577.

40. Costa, M. F.; Costa, M. R. G.; Curto, M. J. M.; Magrinho, M.; Damas, A. M.; Gales, L. *J. Organomet. Chem.* **2001**, *632*, 27–40.
41. Case, D. A.; Darden, T. A.; Cheatham, T. E., III; Simmerling, C. L.; Wang, J.; Duke, R. E.; Luo, R.; Merez, K. M.; Wang, B.; Pearlman, D. A.; Crowley, M.; Brozell, S.; Tsui, V.; Gohlke, H.; Mongan, J.; Hornak, V.; Cui, G.; Beroza, P.; Schafmeister, C.; Caldwell, J. W.; Ross, W. S.; Kollman, P. A. AMBER *version 8*; University of California: San Francisco, 2004.
42. Wang, J.; Wolf, R. M.; Caldwell, J. W.; Case, D. A.; Kollman, P. A. *J. Comput. Chem.* **2004**, *25*, 1157–1174.
43. Jakalian, A.; Bush, B. L.; Jack, D. B.; Bayly, C. I. *J. Comput. Chem.* **2000**, *21*, 132–146.
44. Allen, F. H. *Acta Crystallogr.* **2002**, *B58*, 380–388.
45. Frisch, M. J.; Trucks, G. W.; Schlegel, H. B.; Scuseria, G. E.; Robb, M. A.; Cheeseman, J. R.; Montgomery, J. A.; Vreven, T., Jr.; Kudin, K. N.; Burant, J. C.; Millam, J. M.; Iyengar, S. S.; Tomasi, J.; Barone, V.; Mennucci, B.; Cossi, M.; Scalmani, G.; Rega, N.; Petersson, G. A.; Nakatsuji, H.; Hada, M.; Ehara, M.; Toyota, K.; Fukuda, R.; Hasegawa, J.; Ishida, M.; Nakajima, T.; Honda, Y.; Kitao, O.; Nakai, H.; Klene, M.; Li, X.; Knox, J. E.; Hratchian, H. P.; Cross, J. B.; Bakken, V.; Adamo, C.; Jaramillo, J.; Gomperts, R.; Stratmann, R. E.; Yazyev, O.; Austin, A. J.; Cammi, R.; Pomelli, C.; Ochterski, J. W.; Ayala, P. Y.; Morokuma, K.; Voth, G. A.; Salvador, P.; Dannenberg, J. J.; Zakrzewski, V. G.; Dapprich, S.; Daniels, A. D.; Strain, M. C.; Farkas, O.; Malick, D. K.; Rabuck, A. D.; Raghavachari, K.; Foresman, J. B.; Ortiz, J. V.; Cui, Q.; Baboul, A. G.; Clifford, S.; Cioslowski, J.; Stefanov, B. B.; Liu, G.; Liashenko, A.; Piskorz, P.; Komaromi, I.; Martin, R. L.; Fox, D. J.; Keith, T.; Al-Laham, M. A.; Peng, C. Y.; Nanayakkara, A.; Challacombe, M.; Gill, P. M. W.; Johnson, B.; Chen, W.; Wong, M. W.; Gonzalez, C.; Pople, J. A. *Gaussian 03, Revision C.02*; Gaussian: Wallingford, CT, 2004.
46. Pedretti, A.; Villa, L.; Vistoli, G. *J. Comput.-Aided Mol. Des.* **2004**, *18*, 167–173.
47. Ryckaert, J. P.; Cicotti, G.; Berendsen, H. J. C. *J. Comput. Phys.* **1977**, *23*, 327–341.
48. Delano, W.L. The Pymol Molecular Graphics System, 2002, on World Wide Web http://www.pymol.org.
49. Pettersen, E. F.; Goddard, T. D.; Huang, C. C.; Couch, G. S.; Greenblatt, D. M.; Meng, E. C.; Ferrin, T. E. *J. Comput. Chem.* **2004**, *25*, 1605–1612.